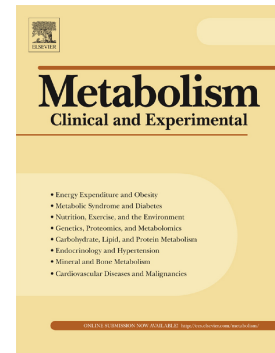


Low-density lipoprotein receptor-related protein 1 deficiency in cardiomyocytes reduces susceptibility to insulin resistance and obesity

Aleyda Benitez-Amaro, Elena Revuelta-López, Olga Bornachea, Lidia Cedo, Àngela Veà, Laura Herrero, Nuria Roglans, Carolina Soler-Botija, David de Gonzalo-Calvo, Laura Nasarre, Sandra Camino-López, J.E. García, Eugenia Mato, Francisco Blanco-Vaca, Antoni Bayes-Genis, David Sebastian, Joan Carles Laguna, Dolors Serra, Antonio Zorzano, Joan Carles Escola-Gil, Vicenta Llorente-Cortes



PII: S0026-0495(20)30055-X

DOI: <https://doi.org/10.1016/j.metabol.2020.154191>

Reference: YMETA 154191

To appear in: *Metabolism*

Received date: 22 August 2019

Accepted date: 24 February 2020

Please cite this article as: A. Benitez-Amaro, E. Revuelta-López, O. Bornachea, et al., Low-density lipoprotein receptor-related protein 1 deficiency in cardiomyocytes reduces susceptibility to insulin resistance and obesity, *Metabolism*(2020), <https://doi.org/10.1016/j.metabol.2020.154191>

This is a PDF file of an article that has undergone enhancements after acceptance, such as the addition of a cover page and metadata, and formatting for readability, but it is not yet the definitive version of record. This version will undergo additional copyediting, typesetting and review before it is published in its final form, but we are providing this version to give early visibility of the article. Please note that, during the production process, errors may be discovered which could affect the content, and all legal disclaimers that apply to the journal pertain.

Low-density lipoprotein receptor-related protein 1 deficiency in cardiomyocytes reduces susceptibility to insulin resistance and obesity

Aleyda Benitez-Amaro,^{1,2#} Elena Revuelta-López,^{3,4#} Olga Bornachea,^{1,2} Lidia Cedo,^{5,6} Àngela Veà,¹ Laura Herrero,^{7,8} Nuria Roglans,⁹ Carolina Soler-Botija,^{3,4} David de Gonzalo-Calvo,^{1,2,4} Laura Nasarre,¹ Sandra Camino-López,¹ García JE,^{1,2} Eugenia Mato^{10,11}, Francisco Blanco-Vaca,^{5,6,12} Antoni Bayes-Genis,^{3,4,13} David Sebastian,^{6,14,15} Joan Carles Laguna,⁹ Dolors Serra,^{7,8} Antonio Zorzano,^{6,14,15} Joan Carles Escola-Gil,^{*5,6} Vicenta Llorente-Cortes,^{*1,2,4}

¹Lipids and Cardiovascular Pathology Group, Biomedical Research Institute Sant Pau (IIB Sant Pau), Barcelona, Spain.

²Institute of Biomedical Research of Barcelona (IIBB) - Spanish National Research Council (CSIC), Barcelona, Spain

³Heart Failure and Cardiac Regeneration (ICREC) Research Program, Health Sciences Research Institute Germans Trias i Pujol (IGTP), Badalona (Barcelona), Spain

⁴Centro de Investigación Biomédica en Red Enfermedades Cardiovasculares (CIBERCV), Instituto de Salud Carlos III, Madrid, Spain

⁵Metabolic Basis of Cardiovascular Risk, Biomedical Research Institute Sant Pau (IIB Sant Pau), Barcelona, Spain

⁶Centro de Investigación Biomédica en Red de Diabetes y Enfermedades Metabólicas Asociadas (CIBERDEM), Instituto de Salud Carlos III, Madrid, Spain

⁷Department of Biochemistry and Physiology, School of Pharmacy, Institut de Biomedicina de la Universitat de Barcelona (IBUB), Universitat de Barcelona, Spain

⁸Centro de Investigación Biomédica en Red Fisiopatología de la Obesidad y Nutrición (CIBEROBN), Instituto de Salud Carlos III, Madrid, Spain

⁹Department of Pharmacology, Toxicology and Therapeutic Chemistry, School of Pharmacy and Food Sciences, Institut de Biomedicina de la Universitat de Barcelona (IBUB), Universitat de Barcelona, Spain.

¹⁰Department of Endocrinology-EDUAB-HSP, Hospital de la Santa Creu i Sant Pau, Barcelona, Spain

¹¹CIBER Bioingeniería, Biomateriales y Nanomedicina, CIBER-BBN, Instituto de Salud Carlos III, Madrid, Spain

¹²Departament de Bioquímica, Biologia Molecular i Biomedicina, Universitat Autònoma de Barcelona, Barcelona, Spain

¹³Cardiology Service and Heart Failure Unit, Hospital Universitari Germans Trias i Pujol, Badalona, Spain. Department of Medicine, Autonomous University of Barcelona, Barcelona

¹⁴Institute for Research in Biomedicine (IRB Barcelona), The Barcelona Institute of Science and Technology, Barcelona, Spain;

¹⁵Departament de Bioquímica i Biomedicina Molecular, Facultat de Biologia, Universitat de Barcelona, Barcelona, Spain.

#These authors contributed equally to this work

*Address correspondence to: Vicenta Llorente-Cortés (CLlorente@santpau.cat; vicenta.llorente@iibb.csic.es) & Joan Carles Escola-Gil (JEscola@santpau.cat), Biomedical Research Institute IIB Sant Pau, IIBB-CSIC, Hospital de la Santa Creu i Sant Pau, Sant Antoni M^a Claret, 167, 08025 Barcelona.

Abstract

Background

Low-density lipoprotein receptor-related protein 1 (LRP1) plays a key role in fatty acid metabolism and glucose homeostasis. In the context of dyslipemia, LRP1 is upregulated in the heart. Our aim was to evaluate the impact of cardiomyocyte LRP1 deficiency on high fat diet (HFD)-induced cardiac and metabolic alterations, and to explore the potential mechanisms involved.

Methods

We used *TnT-iCre* transgenic mice with thoroughly tested suitability to delete genes exclusively in cardiomyocytes to generate an experimental mouse model with conditional *Lrp1* deficiency in cardiomyocytes (*TnT-iCre*⁺-LRP1^{flox/flox}).

Findings

Mice with *Lrp1*-deficient cardiomyocytes (*cm-Lrp1*^{-/-}) have a normal cardiac function combined with a favorable metabolic phenotype against HFD-induced glucose intolerance and obesity. Glucose intolerance protection was linked to higher hepatic fatty acid oxidation (FAO), lower liver steatosis and increased whole-body energy expenditure. Proteomic studies of the heart revealed decreased levels of cardiac pro-atrial natriuretic peptide (pro-ANP), which was parallel to higher ANP circulating levels. *cm-Lrp1*^{-/-} mice showed ANP signaling activation that was linked to increased fatty acid (FA) uptake and increased AMPK/ ACC phosphorylation in the liver. Natriuretic peptide receptor A (NPR-A) antagonist completely abolished ANP signaling and metabolic protection in *cm-Lrp1*^{-/-} mice.

Conclusions

These results indicate that an ANP-dependent axis controlled by cardiac LRP1 levels modulates AMPK activity in the liver, energy homeostasis and whole-body metabolism.

Key Words: Cardiomyocyte, *Lrp1*, ANP, heart, liver, AMPK, fatty acid oxidation

Nonstandard Abbreviations and Acronyms

| | |
|--------------|--|
| ACC | Acetyl-CoA carboxylase |
| Akt | Protein Kinase B |
| AMPK | AMP-activated protein kinase |
| ANP | Atrial natriuretic peptide |
| AUC | Area under the curve |
| BAT | Brown adipose tissue |
| BSA | Phosphate buffered saline |
| BNP | Brain natriuretic peptide |
| CE | Cholesteryl esters |
| cGMP | Cyclic guanosine monophosphate |
| CLAMS | Comprehensive lab animal monitoring system |
| CPT1 | Carnitine palmitoyltransferase I |
| DAPI | 4',6-diamidino-2-phenylindole |
| eWAT | Epididymal fat |
| FA | Fatty acid |
| FAO | Fatty acid oxidation |
| FASP | Filter Aided Sample Preparation |
| FC | Free cholesterol |
| FFA | Free fatty acid |
| GDF15 | Growth and differentiation factor 15 |
| GLUT | Glucose transporter |
| GTT | Glucose tolerance test |
| HDL | High density lipoprotein |
| HF | Heart failure |
| HFD | High fat diet |
| IR | Insulin resistance |
| LDLR | Low density lipoprotein receptor |
| LIPG | Endothelial lipase |
| LpL | Lipoprotein lipase |
| LRP1 | Low-density lipoprotein receptor-related protein 1 |
| LV | left ventricle |
| LVAWd | LV anterior wall at end cardiac diastole |
| LVEDV | LV end-diastolic volume |
| LVEF | LV ejection fraction |
| LVESV | LV end-systolic volume |
| LVFS | LV fractional shortening |

| | |
|--|--|
| LVIDd | LV internal diameter diastole |
| LVIDs | LV internal diameter systole |
| LVPWd | LV posterior wall at end cardiac diastole |
| NP | Natriuretic peptide |
| NPR-A | Natriuretic peptide receptor A |
| NPR-C | Natriuretic peptide receptor C |
| OFG | Oral fat gavage |
| Mitochondrial Oxidative Phosphorylation System | |
| pAMPK | Phosphorylated AMP-activated protein kinase |
| pNpp | p-nitrophenyl phosphate |
| Pro-ANP | Pro-atrial natriuretic peptide |
| Pro-BNP | Pro-brain natriuretic peptide |
| pVASP | Phosphorylated VASP |
| q-RT-PCR | Quantitative real-time reverse transcriptase-polymerase chain reaction |
| RER | Respiratory exchange ratio |
| SCX | Strong Cation Exchange |
| TG | Triglyceride |
| TLC | Thin layer chromatography |
| TMT | Tandem mass tags |
| TnT | Troponin T |
| UCP3 | Mitochondrial uncoupling protein 3 |
| VASP | Vasodilator-stimulated phosphoprotein |
| VCO₂ | CO ₂ production |
| VO₂ | Oxygen consumption |
| VLDLR | Very low-density lipoprotein receptor |
| ZDF | Zucker Diabetic Fatty |

1. Introduction

The metabolic syndrome preceding type 2 diabetes is mainly caused by an inefficient coordination of energy utilization by key organs [1]. It is known that alterations in fatty acid (FA) metabolism play a crucial role in inter-organ dyscoordination and insulin resistance (IR) [2]. Further, in metabolic diseases, the heart shows an exacerbated uptake of free FAs (FFAs) [3] and lipoproteins [4] underlying neutral lipid accumulation in cardiomyocytes.

The low-density lipoprotein receptor-related protein 1 (LRP1) is a key receptor that modulates energy utilization by different tissues. LRP1 is both a carrier and a signaling receptor that regulates processes related with lipid metabolism and glucose homeostasis [5,6]. In the hallmark of lipid metabolism, LRP1 is involved in the uptake of unmodified and modified lipoproteins in different tissues causing alterations in the lipid content, generally associated with dyslipemic conditions. LRP1 is involved in the lipid transport from lipoproteins to hepatocytes [5], coronary vascular smooth muscle cells [7,8], cardiomyocytes [9,10] and adipocytes [11]. Specifically, adipocyte LRP1 modulates not only lipid transport but also glucose homeostasis through the control of insulin sensitivity and energy expenditure [11]. In the context of glucose homeostasis, LRP1 has a regulatory action on the insulin receptor and GLUT4 activation in different tissues and organs including the brain [12,13]. Interestingly, insulin favors LRP1 translocation to the cell membrane in the liver, increasing thus postprandial lipoprotein uptake [14]. Recently, it has been shown that hepatic LRP1 protects against IR and hepatic steatosis [13,15].

The liver plays a central role in the regulation of metabolism, receiving signals from multiple organs such as the pancreatic islets, the central nervous system, adipose tissue and kidneys [16]. It has also been suggested that the heart may also exert control over the metabolism of peripheral organs through the secretion of certain molecules called cardiokines. These cardiokines can affect the metabolic function of various cell types influencing whole-body homeostasis [17–19]. However, it is unknown at this moment whether *lrp1* in cardiomyocytes modulates the production and release of cardiokines potentially involved in whole-body metabolism. The objectives of this study have been to 1) generate a murine experimental model of conditional *Lrp1* deficiency in cardiomyocytes by using the *TnT-iCre* transgenic mice with thoroughly tested suitability to delete genes exclusively in cardiomyocytes [20]; 2) study the impact of cardiomyocyte *Lrp1* deficiency in whole-body metabolism; 3) analyze the differential proteins in the heart of *cm-Lrp1^{-/-}* mice and controls and 4) examine the impact of

differential proteins, in particular of cardiokines, on target-tissue fatty acid uptake and metabolism.

2. Material and methods

***cm-Lrp1*^{-/-} transgenic mice generation and characterization**

We generated an experimental mouse model with conditional and cardiomyocyte-specific *Lrp1* deficiency (TNT-iCre⁺-LRP1^{flox/flox} or *cm-Lrp1*^{+/+}) by treatment with doxycycline [20]. The specific controls for this animal model are TNT-iCre⁻-Lrp1^{flox/flox} or *cm-Lrp1*^{-/-}. The generation of *cm-Lrp1*^{-/-} transgenic mice is described in online Figure S1. To achieve cardiomyocyte-specific LRP1 inactivation, we use a cardiomyocyte-specific Cre deleter and a floxed allele of *Lrp1*. We crossed commercial LRP1^{flox/flox} mice (B6;129S7-Lrp1^{tm2Her}/J; stock: #012604, Jackson Laboratories) carrying loxP sites within the LRP1 gene with TNT-iCre transgenic mice (kindly provided by Prof. Bin Zhou, Albert Einstein College of Medicine, USA) [20], for eight generations (Figure 1A). Transgenic founder mice were genotyped by PCR analysis on tail tip genomic DNA using primers for LRP1, *Cre* and *Nrt* (Figure 1B). Genomic DNA was extracted with a Wizard® SV Genomic DNA Purification System (Promega, Madison, WI, USA) and PCR analysis was performed with oligonucleotides synthesized by IDT (Integrated DNA Technologies, Inc; Coralville, IA, USA), using an Expand High Fidelity PCR System (Roche Molecular Systems). The oligonucleotides used are specified in Table S1.

Mice were housed in specific pathogen-free facilities with a 12-hour light/12-hour dark cycle. Both groups, ten-week-old males *cm-Lrp1*^{+/+} and *cm-Lrp1*^{-/-}, were treated daily with doxycycline cyclate (Sigma-Aldrich) (Dox) through their drinking water (1.5 mg/mL/kg) *ad libitum* to assess the conditional *Lrp1* inhibition in cardiomyocytes. The control group (*cm-Lrp1*^{+/+}) was also treated with Dox to avoid interference with the treatment. Robertson et al., showed that Dox has a long half-life [21].

In the first experimental setting (online Figure S1A), after checking cardiac function, *cm-Lrp1*^{+/+} and *cm-Lrp1*^{-/-} ten-week-old mice were fed high-fat cholesterol-containing diet (HFD TD.88137; Harlan Teklad) for six weeks. In the second experimental setting, *cm-Lrp1*^{+/+} and *cm-Lrp1*^{-/-} ten-week-old mice were randomized to placebo (PBS) or to NPRA antagonist (A71915, 200 µg/Kg in PBS, volume 100 µL) treatment during the 6 weeks on HFD (online Figure S1B). Age-matched littermates were used for all experiments and at least 6 mice per group were analyzed considering $\alpha=0.05$, power=80%, and an effect size of 2 mM glucose and 0.1 µg/L insulin.

Blood samples were taken in fasting conditions in the fourth week (150 μ l) and after sacrificing (400 μ L). The serum was frozen at -20°C and used to measure glucose, insulin and lipid levels. The mice were euthanized at week six and samples from liver, skeletal muscle, heart, epididymal fat (eWAT), and brown adipose tissue (BAT), were kept frozen at -80°C for lipid and molecular analysis. A piece of these tissues was also embedded in OCT for immunohistochemistry. All experimental protocols were approved by the Institutional Animal Care and Use Committees at the Research Institute (IR)-Sant Pau, and complied with all guidelines concerning the use of animals in research and teaching as defined by the Guide for the Care and Use of Laboratory Animals (NIH Publication N^o.80-23, revised 1996).

Biochemical analysis

Insulin serum levels were measured using a Mouse Insulin ELISA (Mercodia) following the manufacturer's instructions. The HOMA index, an estimation of insulin resistance, was calculated as: [fasting serum insulin (ng/ml) x fasting serum glucose (mM)]/22.5. Serum lipids and lipoproteins, including cholesterol, triglyceride (TG) (corrected from free glycerol), phospholipids, FFAs, high density lipoprotein (HDL) cholesterol and phospholipids, were enzymatically determined using commercial kits adapted to a COBAS 6000 autoanalyzer (Roche Diagnostics) [22].

Analysis of ventricular function

Transthoracic echocardiography was conducted under light sedation (1% isoflurane in oxygen) three days after starting doxycycline treatment (baseline). A second echocardiography was conducted six weeks later, at the end of the experimental procedure [23]. Standard functional parameters were measured, including left ventricle (LV) internal diameter diastole (LVIDd) and LV internal diameter systole (LVIDs), LV end-diastolic volume (LVEDV), LV end-systolic volume (LVESV), LV ejection fraction (LVEF), LV fractional shortening (LVFS), LV anterior wall at end cardiac diastole (LVAWd), LV posterior wall at end cardiac diastole (LVPWd), and heart rate.

Glucose tolerance test (GTT)

The glucose tolerance test (GTT) was performed at week six of the dietetic intervention in fasting conditions. Basal blood glucose levels were measured from a tail nick through ACCU-CHEK® Aviva glucometer (Roche Molecular Systems). The mice were then intraperitoneally injected with glucose (1.3mg/g BW). Blood glucose was measured at 15, 30, 60, 120 and 180 min after glucose injection. The area under the

curve (AUC) of the response curve was then calculated using the software Prism 4.0 [24].

Distribution of intragastrically-administered [³H]-TG

Mice were given an oral fat gavage (OFG) consisting of 20 μCi [³H]-labeled triolein (glycerol tri[9, 10(n)-3 H]oleate, 21.0Ci/mmol; Amersham Biosciences, Buckinghamshire, UK) in 150 μL of olive oil [24]. Mice were bled by cardiac puncture at 1.5 hours. Serum and target tissues (liver, eWAT, heart, leg muscle and BAT) were collected after perfusion with NaCl solution 0.9%. Radiolabeled serum and tissue TG were separated from the FA using methanol:chloroform:heptane 1.4:1.25:1 (v:v:v) and 0.1 mol/L $\text{H}_3\text{BO}_3\text{-KCO}_3$ at pH 10.5. The radioactivity in the TG and FA fraction, in total serum and target tissues was determined by scintillation counting.

Cardiomyocyte isolation

Cardiomyocytes were obtained from the heart of our *in vivo* animal model by the Langendorff method. First, the heart was surgically removed and washed with a Ca^{2+} free Tyrode solution at 4°C and oxygenated. The aorta was suspended in the Langendorff apparatus and the heart was perfused via the aorta with Ca^{2+} free Tyrode solution at 37°C to clean blood remnants. The Ca^{2+} free Tyrode solution was then carefully removed, and the enzyme solution composed of Ca^{2+} free Tyrode solution with bovine serum albumin, collagenases and proteinases was added. Two reperfusion cycles (3 ml/min during 6 min) were performed to add the stop solution (Ca^{2+} free Tyrode solution without collagenases and proteinases). Once the perfusion was finished, the heart was removed from the Langendorff system and treated with an enzymatic solution for 5 min at 37°C under shaking. The pieces of tissue were extracted with tweezers and, with shaking, submerged into stop solution to continue disaggregation. Tissue pieces were then removed and the solution containing the cardiomyocytes was centrifuged for 5 min at 450 rpm. The cell pellet was resuspended in stop solution or Tripure™ Isolation Reagent®, depending on the further methodology used.

Tissue homogenization

Frozen tissues (25 mg) (heart, liver, skeletal muscle, eWAT and BAT) were pulverized in liquid nitrogen using a mortar and a pestle. Samples were then homogenized in TriPure™ isolation reagent (Roche Molecular Systems) for total RNA and protein extraction according to the manufacturer's instructions. Total RNA from skeletal muscle

was extracted using the RNeasy mini kit (Qiagen) according to the manufacturer's instructions after the previous addition of Proteinase K. For RNA extraction from eWAT, the tissue was processed with the kit RNeasy Mini Kit (Qiagen). DNA was digested with DNase I (Invitrogen). Extracted RNA was eluted in 25 μ L of nuclease-free water. The yield and quality of RNA was tested by agarose electrophoresis and spectrophotometry. Isolated RNA was stored at -80°C until use.

LRP1-deficient cardiomyocyte cell culture

Murine LRP1-deficient HL-1 cells were generated and kept in culture as previously described [9,10,25,26].

Hepatocyte (Hepa 1-6) cell culture

Hepa 1-6 cells were cultured in DMEM supplemented with 10% FCS, 2 mmol/L L-glutamine, 100 U/mL penicillin G, and 100 $\mu\text{g}/\text{mL}$ streptomycin. Quiescent cells were used for two different experimental approaches. First, quiescent Hepa 1-6 were exposed to supernatants from LRP1- and LRP1- HL-1 cells. Second, quiescent Hepa 1-6 were exposed to increasing dose of ANP (0 to 10 nM).

Gene expression analyses by RT-PCR

Total RNA (1 μg) was used for cDNA synthesis according to the protocol provided with the High Capacity cDNA Reverse Transcription kit (Applied Biosystems). cDNA was stored at -20°C until its use. Gene expression analyses of *Lrp1* (Mm00464608_m1), *Vldlr* (Rn01498166_m1), *Ldlr* (Mm01151339_m1), *Cd36* (Mm01135198-m1), *Nppa* (Mm01255747_g1), *Nppb* (Mm01255770_g1), *Cpt1* (Mm00550438), *Fasn* (Mm00662319_m1), *Acaca* (Mm01304257_m1), *Acs13* (Mm01255804_m1), *Cav1* (Mm00483057_m1), *Slc27a2* (Mm00449517_m1) and *Slc27a4* (Mm01327405_m1) were performed by quantitative real-time reverse transcriptase-polymerase chain reaction (q-RT-PCR) in the Applied Biosystems 7300 Real Time PCR System (Applied Biosystems; Foster City, CA, USA). *18srRNA* (4319413E) was used as a housekeeping gene. The mRNA expression levels were measured in triplicate. The threshold cycle (Ct) values were normalized to the housekeeping gene.

Proteomic studies

Proteomic studies were performed as previously described with small modifications [27,28]. The mass spectrometry proteomics data have been deposited to the ProteomeXchange Consortium via the PRIDE partner repository with the dataset

identifier PXD011564. The protein was digested with Sequencing Grade Modified Trypsin (Promega, Madison, WI, USA) using the FASP (Filter Aided Sample Preparation) digestion protocol as described [27]. A detailed description of the experimental procedures has been included in supplemental material.

Immunoprecipitation Assays

Dynabeads protein G was bound to the polyclonal anti-corin antibody (abcam ab125254) for 1 hour at room temperature. The protein extract was incubated with the Dynabeads Protein G-anti-corin complex overnight at 4°C. After incubation, the protein immune-complex beads were washed 3 times with the wash buffer and eluted with 50 mM glycine. Samples were separated by SDS-PAGE and transferred blots were incubated with Ab against Serpin 1 (biorbyt orb319062).

Corin catalytic activity assay.

Protease corin activity was measured as previously described [29]. Corin activity was presented as V_{max} .

Immunoassays

ANP (ab108797, Abcam), GDF-15 (MGD150, R&D Systems) and adrenalin/epinephrine (abx257158, Abbexa) plasma levels were measured by commercially available-enzyme-linked immunosorbent assays (ELISA), according to the manufacturer's recommendations.

Western blotting analysis

Blots were incubated with antibodies against mouse LRP1 (β -chain, clone 5A6 RDI-PRO61066), AMPK (Cell Signaling Technology, Inc, # 2532), pAMPK (Cell Signaling Technology, Inc, Thr172, 40H9, # 2535), pVASP (Santa Cruz Biotechnology, Inc, sc-101439), BNP (Santa Cruz Biotechnology, Inc, sc-67455), ANP (Everest Biotech, EB11166), Serpin A1 (Biorbyt, orb319062), pACC (Cell Signaling Technology, 1673661S, total ACC (Cell Signaling Technology, 1673662S), pAkt (Cell Signaling Technology, #4060), total Akt (Cell Signaling Technology, #4685), UCP3 (Abcam, ab10985) and OXPHOS mitochondrial complexes (Abcam, ab110413). CPT1 from mitochondrial-enriched fractions in liver was determined [30] using the antibodies described by Herrero L *et al* [31] and registered in antibodyregistry.org (Dolors Serra/Universitat de Barcelona Cat# CPT1A, RRID:AB_2636894). Protein extracts (10

µg) were loaded, resolved on 12% SDS-PAGE and transferred to nitrocellulose membranes (BioRad). Signal detection was carried out with the ECL immunoblotting detection system (GE Healthcare) and the results were quantitatively analyzed using Chemidoc (BioRad). Equal protein loading in each lane was verified by incubating blots with monoclonal antibodies against troponin T (TnT) (Thermo Scientific #MS-295-P) or β-tubulin (Cell Signaling Technology, Inc, #2146).

Measurement of cyclic GMP levels in tissues.

The cyclic guanosine monophosphate (cGMP) levels in heart, liver and skeletal muscle were measured using an ELISA kit according to the manufacturer's instructions for non-acetylated methodology (ADI-900-014, Enzo Life Sciences).

Confocal microscopy

Mouse heart cryosections were subjected to target retrieval (10 mM Tris-HCl, pH=6) and permeabilized with Triton X-100 (0.5%). Isolated cardiomyocytes were fixed with paraformaldehyde and preserved in PBS with sodium acid 0.2%. Cells were permeabilized with glycine (0.1M) and Triton X-100 (0.2%). Samples were blocked with PBS, Tween-20 (0.2%) and BSA (1%) and incubated with primary antibody LRP1 (2 µg/mL Abcam). Secondary antibodies conjugated with Alexa488 and Cy3 (1 µg/mL) (Jackson ImmunoResearch) were used for detection. Cell nuclei were counterstained with 4',6-diamidino-2-phenylindole (DAPI). Results were analyzed with an Axio-Observer Z1 (Zeiss) laser confocal microscope.

Histological staining

Tissue samples were frozen and sectioned (5 µm). Sections were stained with Hematoxylin/Eosin, Herxheimer, Oil red O and Sirius red stains. Herxheimer and oil red O stainings were used for the detection of lipids. A polarized light microscope was used to measure collagen types I and III on randomly selected Sirius red-stained sections.

Lipid extraction and semi-quantitative analysis of cholesteryl ester, free cholesterol, TG and FFA content in target tissues

Frozen pulverized tissue (10 mg) were homogenized in NaOH 0.1 M. Lipids were extracted and cholesteryl esters (CE), free cholesterol (FC) and TG content was analyzed by thin layer chromatography [9,10]. The FFA level was determined enzymatically using commercial kits adapted to a COBAS 6000 autoanalyzer.

Determination of fatty acid β -oxidation (FAO) activity in target tissues

Aliquots from heart and liver were homogenized in a buffer composed of 150 mM NaCl, 1 mM dithiothreitol, 30 mM EDTA and 50 mM KH_2PO_4 . Tissue fatty acid oxidation (FAO) was determined with 30 μg of post nuclear supernatant by determining the conversion of palmitoyl CoA-1- ^{14}C into acetyl-CoA [32].

Indirect Calorimetry System

Measurements of oxygen consumption (VO_2) and CO_2 production (VCO_2) were performed using a comprehensive lab animal monitoring system (Oxymax-CLAMS, Columbus Instruments). Mice were acclimated in metabolic chambers for 1 day before the start of the recordings. Animals were continuously recorded for 2 days with measurements of their locomotor activity (in the xy and z axes) and gas exchange (O_2 and CO_2) taken every 20 min. Energy expenditure was calculated according to manufacturer's guidelines (Columbus Instruments). The respiratory quotient was estimated by calculating the ratio of CO_2 production to O_2 consumption.

Statistical analysis

Results are expressed as mean \pm SEM. Differences between study groups were analyzed using one-way analysis of variance (ANOVA) followed by a *post-hoc Tukey-b* test, Student's *t*-test for independent samples and Student's *t*-test for paired samples. The statistical software R (www.r-project.org) was used for all statistical analyses. Differences were considered statistically significant when $P < 0.050$.

3. Results

3.1. Cardiomyocyte *Lrp1* Deficiency Prevents Diet-Induced Overweight and Glucose Intolerance By Facilitating Increased Energy Expenditure

Cardiomyocyte *Lrp1* deficient (*cm-Lrp1*^{-/-}) mice were generated as explained in section 2.1 using the *TnT-iCre* transgenic mice provided by Zhou and Bu [20]. These authors showed that the transgenic method they used to generate *TnT-iCre* transgenic mice guarantees the deletion of genes exclusively in cardiomyocytes through all the states of heart development. Here, we investigated the effects of *Lrp1* specific deletion in cardiomyocytes by crossing *TnT-iCre* transgenic mice with *Lrp1*^{fllox/fllox} that generated *cm-lrp1*^{-/-} mice. A schematic representation of *cm-Lrp1*^{-/-} generation and genotyping is shown in Figure 1A,B. *cm-Lrp1*^{-/-} mice fed either chow or HFD diet showed decreased

Lrp1 levels in isolated cardiomyocytes and in the heart (Figure 1C-E). However, no differences were found in other lipoprotein receptors including *vldlr* or *ldlr* in the heart of *cm-Lrp1*^{-/-} and control mice (*online* Figure S2A). *Lrp1* levels in liver, skeletal muscle and eWAT did not show differences between *cm-Lrp1*^{-/-} and control mice (*online* Figure S2B-D).

First, we evaluated the effects of cardiomyocyte-specific Cre deleter on *Lrp1* expression in chow-fed animals treated with doxycycline. These mice usually exhibit moderate increases in weight and IR when fed a chow diet, but sharp increases when fed a Western-type diet [22]. Surprisingly, the body weight of *cm-Lrp1*^{-/-} mice was lower than that of the controls when the animals were fed a chow diet for a period of 6 weeks and this was concomitant with lower insulin levels and improved glucose tolerance as well as lower hepatic fat accumulation and eWAT weight (*online* Figure S3A-F). Thus, we used western diet-fed *cm-Lrp1*^{-/-} mice to evaluate a putative role of cardiomyocyte *Lrp1* deficiency on metabolic phenotype and the potential mechanisms involved. *Lrp1* deficiency did not cause significant alterations in functional or structural properties of the heart (*online* Figure S4 and S5) or in serum lipid profile (*online* Table S2).

The body weight of *cm-Lrp1*^{-/-} mice was lower than that of the controls at all tested times (Figure 2A) while the average weekly food intake was similar between both groups (*online* Figure S6). This suggests that the reduction in body weight gain was not due to differences of weekly food consumption. The weight-reducing effect of *Lrp1* deficiency was associated to decreased eWAT weight and eWAT/BAT adipocyte size (Figure 2A-C). While TG/FA content was reduced in the liver of *cm-Lrp1*^{-/-} mice (Figure 2D), no differences were found in the heart and skeletal muscle of both groups (*online* Figure S7). To know whether these phenotypic changes elicit a favorable metabolic profile, we conducted a TTG test. Compared with controls, *cm-Lrp1*^{-/-} mice had lower glucose intolerance and lower AUC values (Figure 2E). Glucose, insulin and IR index (HOMA-IR) were reduced in *cm-Lrp1*^{-/-} compared to control mice (Table 1).

To determine whether cardiomyocyte *Lrp1* deficiency reduces body weight and adiposity by regulating energy expenditure, we performed Comprehensive Lab Animal Monitoring System (CLAMS) experiments. These experiments showed that the ambulation activity was higher during the dark period than during the light period. There were, however, no differences between *cm-Lrp1*^{-/-} and control mice (*online* Figure S8), indicating that the protection against weight gain of *cm-Lrp1*^{-/-} mice was not caused by increased physical activity. *cm-Lrp1*^{-/-} mice showed higher lipid oxidation

during the light phase (Figure 3A) and higher glucose oxidation during the dark phase (Figure 3B). *cm-Lrp1^{-/-}* mice showed higher VO₂ and energy expenditure than controls during both phases (Figure 3C & D).

3.2. Hearts with *Lrp1* Deficiency Show Enhanced Corin Activity That Favors Higher ANP Release to the Plasma

To identify cardiac proteins potentially involved in the favorable metabolic phenotype of *cm-Lrp1^{-/-}* mice, we performed proteomic analysis of hearts from both *cm-Lrp1^{-/-}* and *cm-Lrp1^{+/+}* mice groups. We processed three biological replicates from each group. Each replicate was a pool from three animals. We identified 24,358 spectra corresponding to 6,334 non-redundant peptides through a database search (1% FDR) (Data is available via the ProteomeXchange with the identifier PXD011564). For quantitative analysis, only peptides identified as unique (i.e. peptides sequences belonging to one single protein in the database) were considered. Overall, a total of 1,213 proteins were quantified from 5,735 non-redundant unique peptides. Quantified proteins were compared between groups and we found a total of 34 differential expressed proteins. These 34 proteins included 11 which have the potential to be secreted (Table 2). Among the differential secreted proteins, we found atrial natriuretic peptide (ANP) (ratio=0.58; p=2.1E-04) and serine protease inhibitors including serpin1a (ratio=0.71; p=2.0E-12), serpin 1b (ratio=0.54; p=6.0E-05), serpin 1d (ratio=0.33; p=1.7-E-03) and serpin 3K (ratio=0.71; p=4.0E-09). To validate the Proteomics results, Western blot and immunoprecipitation experiments were performed.

As shown in Figure 4A, ANP is generated from the precursor form proANP through the activation of corin, a convertase that facilitates the release of ANP (28 aa) from the C-terminal end of proANP [33]. Western blot analysis performed with Abs that bind to the sequence RIGAQSGLCNSFR at the C-terminal end of precursor form showed that proANP (14 kDa) levels were strongly decreased in *cm-Lrp1^{-/-}* compared to control mice. This same test also showed preproANP (17 kDa) to be similar among the groups (Figure 4B). These results confirm proteomic differences (decreased levels of proANP in hearts from *cm-Lrp1^{-/-}* mice) and suggest that there is higher release of ANP from LRP1- hearts.

Immunoprecipitation studies evidenced that serpins form complexes with corin. The number of SerpinA1/Corin complexes were higher in the heart of *cm-Lrp1^{-/-}* mice compared to that of controls (Figure 4C). The molecular weight of these complexes in

the heart of our murine model was 45-50 KDa and 30-35 KDa, which lines up with what was previously described of cultured cardiomyocytes [34]. Gladysheva IP *et al* reported that serpin1 binding to corin creates steric impediments to the union of effective inhibitors and allows prolonged corin activation [34].

Fluorogenic assays performed in this study revealed that protease enzymatic activities were higher in the cardiac membranes of *Lrp1*^{-/-} mice with or without hirudin (Figure 4D). Hirudin, a highly specific thrombin inhibitor, was added to the assay to exclude clotting enzymes in the membrane fraction. It did not show a significant effect on protease activity, suggesting that corin could be one of the main proteases contributing to the higher protease activity in cardiac membranes of *Lrp1*^{-/-} mice.

Circulating ANP levels were higher (about 4-fold) in the plasma of *cm-Lrp1*^{-/-} than in that of *cm-Lrp1*^{+/+} mice (Figure 4E). Our results suggest that cardiac *Lrp1* deficiency facilitates corin activation and ANP release. There were no differences in cardiac *Nppa* between groups, whereas a modest downregulation in *Nppb* mRNA expression was found in *cm-Lrp1*^{-/-} mice (*online* Figure S9). No differences were found in the circulating levels of other metabolic factors including adrenalin/epinephrine and GFD15 (Figure 4F,G).

3.3. The ANP-NPR-A Signaling Activation Is Linked To AMPK Phosphorylation and Increased FA Oxidation in the Liver of *cm-Lrp1*^{-/-} Mice

To ascertain whether increased circulating ANP levels were associated with the activation of NPR-A signaling in peripheral tissues, we determined the levels of crucial mediators such as cGMP and pVASP in the liver, skeletal muscle and heart of *cm-Lrp1*^{+/+} and *cm-Lrp1*^{-/-} mice whether treated with the NPR-A antagonist A71915 or not (*online* Figure S1B). cGMP and VASP were increased in the liver (Figure 5A,B) and skeletal muscle (*online* Figure S10A,B) but not the heart (*online* Figure S11A,B) of untreated *cm-Lrp1*^{-/-} mice. The treatment of *cm-Lrp1*^{-/-} mice with A71915 completely blocked the increase of cGMP and pVASP levels in liver and partially blocked it in skeletal muscle. We found that cGMP/pVASP signaling was linked to increased AMPK phosphorylation in the liver. Increased levels of hepatic pAMPK, like those of cGMP and pVASP, were abolished by the NPR-A antagonist (Figure 5A,B). There were no differences in pAMPK levels in the skeletal muscle (*online* Figure S10B) or the heart (*online* Figure S11B) between groups. To know whether AMPK phosphorylation was linked to AMPK activity, we measured the phosphorylation of ACC, the downstream target of pAMPK. ACC mRNA expression levels in the liver of mice fed HFD were

extremely low (reduced by approx. 90% in HFD fed mice). Despite this, we detected an increased ratio pACC/total ACC in the liver of untreated *cm-Lrp1^{-/-}* compared to the control mice (Figure 5A). In addition, the increase in the phosphorylation of ACC was not observed in A91915-treated mice, supporting the activation of AMPK by ANP in the liver of KO mice. To explore the potential impact of pAMPK activation on hepatic FA synthesis, we explored several genes involved in FA synthesis in the liver. We found that *Acs/3* mRNA expression was significantly lower in the liver of KO mice compared to the controls (*online* Figure S12). There were no differences in the mRNA expression levels of *Fasn* or *Slc27a2* between groups.

To know the impact of pAMPK on FAO, we measured CPT1, a key mitochondrial enzyme responsible for FAO; the main components of the oxidative phosphorylation system (OXPHOS), responsible for mitochondrial respiration; and UCP3, an indicator of mitochondrial response to enhanced intracellular FA. Oxidative phosphorylation involves a flow of electrons through the electron transport chain (ETC), a series of proteins and electron carriers within the mitochondrial membrane. We used one OXPHOS cocktail antibody that contains 5 mouse Abs and detects one subunit of each (five) mitochondrial complexes of the ETC. The main subunits detected in whole hepatic and skeletal muscle tissue extracts of our murine model were CV-ATP5A (55 kDa), CIII-UQCRC2 (48 kDa) and CII-SDHB (30 kDa). The protein levels of CPT1, CII, and CV subunits of ETC were significantly higher in the liver (Figure 5C) of untreated KO mice. The increase in these mitochondrial proteins was abolished in *cm-Lrp1^{-/-}* mice treated with A71915, indicating that NPRA-signaling is involved in the increase of OXPHOS protein subunits in mice. UCP-3, an indicator of FA supply to mitochondria, was also induced in the liver (Figure 5C) but not in the skeletal muscle (*online* Figure S10C) of KO mice. These results suggest that, despite the upregulatory effect of ANP signaling on OXPHOS subunits of the skeletal muscle, ANP signaling is not linked to FA oxidation in the skeletal muscle.

According to CPT1 upregulation, the hepatic FAO activity was higher in untreated KO mice than in control mice, but this increase was not observed in KO mice treated with A71915 (Figure 5D). In addition, KO mice showed reduced hepatic TG accumulation in the untreated mice but not in the A71915-treated mice (Figure 5E).

To explore whether these favorable changes may influence insulin signaling activation, we measured the activation state of Akt in different tissues. We found an increased ratio of pAkt/total Akt exclusively in the liver of KO mice (*online* Figure S13).

3.4. Supernatants from LRP1 deficient HL-1 Cells Increased pAMPK and CPT1 Levels in Cultured Hepatocytes

LRP1-deficient HL-1 cells (LRP1-) were generated in our group and previously used to test the impact of the cardiomyocyte LRP1 deficiency in several processes [9,10,25,26]. LRP1- cells show almost undetectable levels of LRP1 but similar morphologic characteristics to the control cells (Figure 6A,B). Supernatants from LRP1- cells contain higher ANP levels than those from control cells (Figure 6C), and, when added to hepatocytes, caused induced AMPK phosphorylation and increased CPT1 protein levels in cultured Hepa 1-6 cells (Figure 6D,E). In parallel experiments, we also showed that ANP from 0 to 10 nM caused an increase in pAMPK/AMPK ratio and CPT1 protein levels in a dose-response manner without altering cell morphology (*online* Figure S14A-C).

3.5. Activated ANP-NPR-A Signaling Is Linked to Increased FA Uptake by the Liver

AMPK phosphorylation has been previously reported to activate FA uptake in oxidative tissues [35,36]. Oral fat gavage (OFG) experiments showed an increase in [³H]-TG and [³H]-FFA uptake by the liver of *cm-Lrp1^{-/-}* mice that was blocked by the NPR-A antagonist A71915 (Figure 7A). Real-time PCR experiments showed an increased expression of hepatic *Vldlr* and *Cd36* mRNA in *cm-Lrp1^{-/-}* mice (Figure 7C) that were also efficiently blocked by the NPR-A antagonist. Unlike the liver, there were no differences between KO and control mice in [³H]-TG and [³H]-FFA uptake by the skeletal muscle, although a significant increase in [³H]-TG and [³H]-FFA uptake was detected in groups treated with A71915 (*online* Figure S15). In contrast to liver, there was a reduced uptake of [³H]-TG and [³H]-FFA by eWAT of *cm-Lrp1^{-/-}* mice (Figure 7B). Reduced levels of *Vldlr* and *Cd36* mRNA expression was detected in eWAT of KO *versus* control mice (Figure 7D). As shown in Figure 7E,F, A71915 equaled eWAT weight and eWAT adipocyte size between *cm-Lrp1^{-/-}* and *cm-Lrp1^{+/+}* mice.

CLAMS experiments showed that treatment of *cm-Lrp1^{-/-}* mice with the NPR-A antagonist counteracted increased lipid oxidation during the light phase (Figure 8A) and increased glucose oxidation during the dark phase (Figure 8B). There were no differences in oxygen consumption (Figure 8C) and energy expenditure (Figure 8D) between *cm-Lrp1^{-/-}* and control mice treated with the NPR-A antagonists.

4. Discussion

The main innovative findings of this study are that LRP1 receptor levels in cardiomyocytes regulate circulating levels of atrial natriuretic peptide and that through this mechanism control NPRA-dependent fatty acid metabolism in the liver and, consequently, the whole-body metabolism.

LRP1 Controls the Systemic Levels of Atrial Natriuretic Peptide through Modulation of Corin Activity in Cardiomyocytes

Here, we show that isolated cardiomyocytes from *cm-Lrp1*^{-/-} mice are deficient in the receptor *Lrp1*. Previous studies have shown that LRP1 plays a crucial role in the degradation of serpin:protease complexes [37,38]. Results from the immunoprecipitation assays performed in this study indicated that corin, the main protease responsible for cardiac release of atrial natriuretic peptide [33], was mostly complexed with serpins in the heart of *cm-Lrp1*^{-/-} mice, as it was previously shown in cultured cardiomyocytes [34]. In agreement with the capacity of LRP1 to modulate protease levels, we found that *Lrp1* deficiency in the cardiomyocyte, the most abundant and main ANP producing cell in the heart [39,40], directly impacts corin activity, cardiac ANP release and ANP circulating levels. A more direct proof of the capacity of LRP1 to modulate ANP release has been obtained from cell culture experiments performed with an LRP1-deficient HL-1 cell line (LRP1- HL-1 cells) previously generated in our group [9,10,25,26]. Our results evidenced the presence of higher ANP levels in the supernatants from LRP1- HL-1 cells compared to control cells.

The protease corin is also involved in the cleavage of pro-brain natriuretic peptide (BNP) to BNP [41]. Despite this, we did not observe alterations in cardiac or plasma BNP levels in *cm-Lrp1*^{-/-} mice compared to the controls. The specific effect of the receptor deficiency on ANP release could be explained by the predominance of ANP (compared to the marginal presence of BNP) in hearts without ventricular dysfunction [42].

Several groups including ours, have determined that the modulation of *Lrp1* receptor causes alterations of key signaling pathways in the heart. Our group reported that cardiac *Lrp1* overexpression contributes to enhanced cholesterol and triglyceride supply to the heart and is associated with serious calcium-handling alterations [25]. In the context of the myocardial infarction, LRP1 signaling activation has been reported to induce a cardioprotective signal, decreases infarct size, and preserves cardiac systolic function in young adult mice without comorbidities [43]. Elevated levels of *Lrp1* ligands, such as VLDL, can act as antagonists of *Lrp1* signaling [44]. Results from the present

study show that cardiomyocyte *Lrp1* deficiency did not affect in cardiac function. This could be related to the absence of pathological stressors such as atherogenic dyslipemia or hypoxia. Further studies are required to know the optimal *Lrp1* threshold values in the presence of certain pathological ligands

ANP Activates NPR-A Signaling That Is Linked to AMPK Phosphorylation and Increased FA Oxidation/FA Uptake in the Liver of *cm-Lrp1*^{-/-} Mice.

The systemic effects of ANP are well described, contributing to water-salt balance maintenance and blood pressure regulation through diuretic, natriuretic and vasodilatory effects. In addition, ANP displays important pleiotropic effects in the heart, acting as a main regulator of cardiovascular homeostasis in an autocrine and paracrine manner [45]. Besides the hemodynamic effects, ANP also is involved in lipolytic processes in white adipose tissue in primates [46]. Recently, it has been described as a potent lipolytic agent that exerts a great impact on the metabolism of patients with heart failure [47]. Interestingly, ANP induces anti-inflammatory effects in adipose tissue [48].

ANP has also been reported to promote oxidative metabolism in human skeletal muscle. In particular, ANP induces PGC-1 α and mitochondrial OXPHOS gene expression in a cyclic GMP-dependent manner in human myotubes [49]. Results from the present study show that ANP increased NPR-A/cGMP/pVASP in the skeletal muscle of *cm-Lrp1*^{-/-} mice. In our murine model, this upregulatory effect of ANP signaling was linked to mitochondrial OXPHOS upregulation, affecting CV-ATP5A and CII-SDHB subunit overexpression. However, there were no differences in the levels of phosphorylated AMPK, the TG/FA uptake, the levels of CPT1 and UCP3, and TG accumulation in the skeletal muscle of *cm-Lrp1*^{-/-} and control mice. These results indicate that FA uptake and FA oxidation were not significantly modulated by NPR-A/cGMP/pVASP signaling in the skeletal muscle of *cm-Lrp1*^{-/-} mice.

In contrast, we found that NPR-A/cGMP/pVASP signaling was linked to AMPK phosphorylation in the liver of *cm-Lrp1*^{-/-} mice. Our cell culture experiments evidenced that hepatocytes exposed to supernatants from LRP1- HL-1 cells or to ANP directly showed increased levels of phosphorylated AMPK. Previous studies have shown that pVASP, an ANP signaling mediator, phosphorylated specifically AMPK in the liver of a mouse model of diabetes [50]. AMPK is considered the master regulator of lipid metabolism and mitochondrial homeostasis [51–54]. One of the crucial functions of AMPK is the regulation of lipid metabolism through the phosphorylation of ACC. Upon

activation of AMPK, phosphorylation of ACC results in ACC inactivation. Our results indicate that ACC phosphorylation is increased in the liver of KO mice and abolished by the treatment of KO mice with the NPR-A antagonist, indicating that the energy sensing AMPK/ACC pathway can be modulated by ANP in the liver. *Acs/3* mRNA expression levels were also decreased in the liver of *cm-Lrp1^{-/-}* compared to control mice. *Acs/3* knockdown decreased total acyl-CoA synthetase activity in *ob/ob* mice and mice fed a high sucrose diet [55]. Together, these results support that ANP-induced AMPK phosphorylation is involved in the deactivation of FA synthesis in the liver of *cm-Lrp1^{-/-}* mice.

The phosphorylation of ACC inhibits the production of malonyl-CoA, a substrate for fatty acid synthase (FAS) and a potent inhibitor of CPT1 [56]. CPT1 is the main mitochondrial enzyme responsible for fatty acid oxidation. Results from the present study showed increased levels of CPT1 in the liver *cm-Lrp1^{-/-}* mice and in hepatocytes exposed to increased ANP levels. We also showed that this increase is dependent of NPR-A signaling. The link between AMPK phosphorylation and CPT1 activation has been previously shown in oxidative tissues of a mice model [36,51]. The upregulation of the mitochondrial OXPHOS subunits support and enhanced mitochondrial respiration in the liver of *cm-Lrp1^{-/-}* mice. Further experiments are required to know the mechanism by which ANP signaling enhances the level of these OXPHOS protein subunits. This could be due to enhanced mitochondrial synthesis or enhanced amount of protein subunits per mitochondria. Together these results support an ANP-enhanced mitochondrial fatty acid oxidation in the liver of *cm-Lrp1^{-/-}* mice.

Finally, UCP3, an indicator of mitochondrial response to intracellular FA, [³H]-FA and [³H]-TG uptake and FA/TG transporters such as Cd36 and VLDLR were upregulated in the liver of KO mice and the increase was abolished by the treatment of KO mice with the NPR-A antagonist. Previous studies have reported that pAMPK positively modulates *Cd36* in a mouse model of AMPK activation specifically in the liver [57]. Together, these results evidenced that ANP signaling promoted by cardiomyocyte LRP1 deficiency facilitates the repression of FA synthesis and the activation of FA uptake/FA mitochondrial oxidation in an AMPK-coordinated manner in the liver of *cm-Lrp1^{-/-}* mice.

ANP-Induced Hepatic FAO Confers a Favorable Metabolic Profile to *cm-Lrp1^{-/-}* Mice

Here, we show that enhanced FA uptake and oxidation promoted by ANP reduces TG accumulation in the liver of KO mice. These results are in agreement with previous studies showing that moderate increases in *Cpt1a* activity are sufficient to reduce hepatic TG levels in CPT-1a-overexpressing animals [58] and even to modulate diabetes and obesity [30]. Interestingly, reduced hepatic triglyceride content in KO mice occurred in the context of enhanced supply of FA to the liver, and, by counteracting ANP-induced FA uptake by the liver, the NPR-A antagonist caused an increased FA uptake by eWAT. Although, a direct effect of ANP on adipose tissue of *cm-Lrp1^{-/-}* cannot be discarded, data from the present study supports the secondary nature of cardiac *Lrp1* deficiency's benefits such as reducing diet-induced obesity and increasing energy expenditure. The liver is considered the main organ in the homeostasis of lipids and glucose and one of the highest contributors to whole-body lipid oxidation [59]. Moreover, previous studies have consistently demonstrated the link between the hepatic FAO and insulin-resistance [45,47,54]. Results from the present study show that phosphorylation of Akt, a crucial step in the insulin signaling pathway, is more active in the liver of *cm-Lrp1^{-/-}* mice compared with controls. In addition, CLAMS experiments showed an ANP-induced glucose oxidation during the dark phase. However, further studies based on the analysis of signaling right after insulin administration are indeed required to obtain conclusions about the role of ANP on the modulation of diet-induced hepatic insulin resistance [60]. Similarly, it would be interesting to determine whether the response to leptin is altered in our model.

Main Conclusions and Translational Potential of the Work

Our results show that the favorable metabolic profile and increased energy expenditure in *cm-Lrp1^{-/-}* mice mainly depends on ANP signaling involving hepatic AMPK activation (summarized in Figure 9).

From the clinical point of view, our team has evaluated natriuretic peptide levels in patients with chronic heart failure. Recently, we described that patients with a low capacity to degrade active natriuretic peptides had better outcomes [61,62]. In humans, the main protective metabolic effects of ANP are related to ANP lipolytic effects in adipose tissue [46,63–67]. In fact, high levels of natriuretic peptides in plasma have been associated with weight loss in humans [66,67]. Here, treatment of *cm-Lrp1^{-/-}* mice with the NPR-A antagonist restores energy expenditure to the levels of control mice, suggesting that ANP/NPR-A signaling is involved in the increased energy expenditure and reduced weight of *cm-Lrp1^{-/-}* mice. It will be interesting to test in humans whether ANP-induced hepatic FA uptake/oxidation is an additional mechanism contributing to the impact of high circulating NP levels in weight loss. According to the present study,

low levels of *Lrp1* expression in cardiomyocytes would contribute to the maintenance of elevated NP levels in circulation. This could be highly relevant in patients with metabolic disorders.

Acknowledgements

The authors thank Dr. Bin Zhou and Dr. Bingruo Wu (Department of Genetics, Albert Einstein College of Medicine, New York, USA) for kindly providing the Tnt2-Cre line, Dra. Montserrat Carrascal (CSIC Proteomics Unit) for her valuable help with the interpretation and representation of Proteomic data and Dr. Marta Casado (Instituto BioMedicina Valencia, CSIC) for help with line management and embryo preservation.

Funding

This work was funded by FIS PI14/01729 and FIS PI18/01584 (to VLI-C), FIS16/00139 (to JCE-G) grants from Instituto Salud Carlos III, co-financed by the European Fund for Regional Development (E.F.R.D.) and by the Ministry of Spain-MINECO (SAF2014-52223-C2-1-R to DS, co-financed by the European Fund for Regional Development (E.F.R.D.)). Support was received from Ministerio de Economía y Competitividad to DdG-C (IJCI-2016-29393), Agència de Gestió d'Ajuts Universitaris i de Recerca Grant FI to ERL (FI-DGR 2013/00014), Fundació MARATÓ TV3 Project 201521-10 (to VLI-C) and Project 87/C/2016 to DS. CIBER Diabetes y Enfermedades Metabólicas Asociadas (CIBERDEM; CB07/08/0016 (FBV, JCE-G, LC); CB07/08/0017 (AZ), CIBER Fisiopatología de la Obesidad y la Nutrición (CIBEROBN; CB06/03/0001 (DS, LH); CB06/03/0017 (JCL, NR)) and CIBER Enfermedades Cardiovasculares (CIBERCV; CB16/1100403 (DdG-C, VLI-C, CS, ERL and AB-G) are Instituto de Salud Carlos III (ISCIII) projects .

Conflicts of interest

The authors have declared no potential conflicts of interest.

Concept and design: Vicenta Llorente-Cortés and Joan Carles Escola-Gil.

Performed the experiments: Aleyda Benítez-Amaro, Elena Revuelta-López, Olga Bornachea, Lidia Cedo, Angela Veá, Laura Herrero, Nuria Roglans, Carolina Soler-Botija, Laura Nasarre, David Sebastian.

Data analysis and interpretation: Vicenta Llorente-Cortés, David de Gonzalo-Calvo, Sandra Camino-López, Francisco Blanco Vaca, Antoni Bayes Genis, Antonio Zorzano, Joan Carles Laguna, Dolors Serra, Joan Carles Escola-Gil, David Sebastian.

Writing and review of Manuscript: Elena Revuelta-López, Joan Carles Escola-Gil, Vicenta Llorente-Cortés.

References

- [1] Grundy SM, Pasternak R, Greenland P, Smith S, Fuster V. Assessment of Cardiovascular Risk by Use of Multiple-Risk-Factor Assessment Equations : A Statement for Healthcare Professionals From the American Heart Association and the American College of Cardiology. *Circulation* 1999;100:1481–92. doi:10.1161/01.CIR.100.13.1481.
- [2] Goldberg IJ. Diabetic Dyslipidemia: Causes and Consequences. *J Clin Endocrinol Metab* 2014;86:965–71. doi:10.1210/jcem.86.3.7304.
- [3] Kankaanpää M, Lehto HR, Pärkkä JP, Komu M, Viljanen A, Ferrannini E, et al. Myocardial triglyceride content and epicardial fat mass in human obesity: Relationship to left ventricular function and serum free fatty acid levels. *J Clin Endocrinol Metab* 2006;91:4689–95. doi:10.1210/jc.2006-0584.
- [4] Pillutla P, Hwang YC, Augustus A, Yokoyama M, Yagyu H, Johnston TP, et al. Perfusion of hearts with triglyceride-rich particles reproduces the metabolic abnormalities in lipotoxic cardiomyopathy. *Am J Physiol Metab* 2005;288:E1229–35. doi:10.1152/ajpendo.00273.2004.
- [5] Moon JH, Kang SB, Park JS, Lee BW, Kang ES, Ahn CW, et al. Up-regulation of hepatic low-density lipoprotein receptor-related protein 1: A possible novel mechanism of antiatherogenic activity of hydroxymethylglutaryl-coenzyme A reductase inhibitor: Atorvastatin and hepatic LRP1 expression. *Metabolism* 2011;60:930–40. doi:10.1016/j.metabol.2010.08.013.
- [6] Dato VA, Chiabrando GA. The role of low-density lipoprotein receptor-related protein 1 in lipid metabolism, glucose homeostasis and inflammation. *Int J Mol Sci* 2018. doi:10.3390/ijms19061780.
- [7] Llorente-Cortés V, Martínez-González J, Badimon L. LDL receptor-related protein mediates uptake of aggregated LDL in human vascular smooth muscle cells. *Arterioscler Thromb Vasc Biol* 2000;20:1572–9. doi:10.1161/01.ATV.20.6.1572.
- [8] Llorente-Cortés V, Otero-Viñas M, Badimon L. Differential Role of Heparan Sulfate Proteoglycans on Aggregated LDL Uptake in Human Vascular Smooth Muscle Cells and Mouse Embryonic Fibroblasts. *Arterioscler Thromb Vasc Biol* 2002;22:1905.

- [9] Cal R, Juan-Babot O, Brossa V, Roura S, Gálvez-Montón C, Portoles M, et al. Low density lipoprotein receptor-related protein 1 expression correlates with cholesteryl ester accumulation in the myocardium of ischemic cardiomyopathy patients. *J Transl Med* 2012;10. doi:10.1186/1479-5876-10-160.
- [10] Cal R, Castellano J, Revuelta-Lpez E, Aledo R, Barriga M, Farr J, et al. Low-density lipoprotein receptor-related protein 1 mediates hypoxia-induced very low density lipoprotein-cholesteryl ester uptake and accumulation in cardiomyocytes. *Cardiovasc Res* 2012;94:469–79. doi:10.1093/cvr/cvs136.
- [11] Hofmann SM, Zhou L, Perez-Tilve D, Greer T, Grant E, Wancata L, et al. Adipocyte LDL receptor-related protein-1 expression modulates postprandial lipid transport and glucose homeostasis in mice. *J Clin Invest* 2007;117:3271–82. doi:10.1172/JCI31929.
- [12] Bogan JS. Regulation of Glucose Transporter Translocation in Health and Diabetes. *Annu Rev Biochem* 2012. doi:10.1146/annurev-biochem-060109-094246.
- [13] Ding Y, Xian X, Holland WL, Tsai S, Herz J. Low-Density Lipoprotein Receptor-Related Protein-1 Protects Against Hepatic Insulin Resistance and Hepatic Steatosis. *EBioMedicine* 2016;7:135–45. doi:10.1016/j.ebiom.2016.04.002.
- [14] Laatsch A, Merkel M, Talmud PJ, Grewal T, Beisiegel U, Heeren J. Insulin stimulates hepatic low density lipoprotein receptor-related protein 1 (LRP1) to increase postprandial lipoprotein clearance. *Atherosclerosis* 2009;204:105–11. doi:10.1016/j.atherosclerosis.2008.07.046.
- [15] Jeon BH, Lee YH, Yun MR, Kim SH, Lee BW, Kang ES, et al. Increased expression of ATP-binding cassette transporter A1 (ABCA1) as a possible mechanism for the protective effect of cilostazol against hepatic steatosis. *Metabolism* 2015. doi:10.1016/j.metabol.2015.07.014.
- [16] Bergman RN, Piccinini F, Kabir M, Ader M. Novel aspects of the role of the liver in carbohydrate metabolism. *Metabolism* 2019. doi:10.1016/j.metabol.2019.05.011.
- [17] Nakamura M, Sadoshima J. Heart over mind: metabolic control of white adipose tissue and liver. *EMBO Mol Med* 2014;6:1521–4. doi:10.15252/emmm.201404749.

- [18] Shimano M, Ouchi N, Walsh K. Cardiokines: Recent progress in elucidating the cardiac secretome. *Circulation* 2012;126. doi:10.1161/CIRCULATIONAHA.112.150656.
- [19] Planavila A, Fernández-Solà J, Villarroya F. Cardiokines as Modulators of Stress-Induced Cardiac Disorders. *Adv. Protein Chem. Struct. Biol.*, vol. 108, 2017, p. 227–56. doi:10.1016/bs.apcsb.2017.01.002.
- [20] Wu B, Zhou B, Wang Y, Cheng HL, Hang CT, Pu WT, et al. Inducible cardiomyocyte-specific gene disruption directed by the rat *Tnnt2* promoter in the mouse. *Genesis* 2010;48:63–72. doi:10.1002/dvg.20573.
- [21] Robertson A, Perea J, Tolmachova T, Thomas PK, Huxley C. Effects of mouse strain, position of integration and tetracycline analogue on the tetracycline conditional system in transgenic mice. *Gene* 2002;282:65–74. doi:10.1016/S0378-1119(01)00793-4.
- [22] Escolà-Gil JC, Llaverias G, Julve J, Jauhiainen M, Méndez-González J, Blanco-Vaca F. The cholesterol content of western diets plays a major role in the paradoxical increase in high-density lipoprotein cholesterol and upregulates the macrophage reverse cholesterol transport pathway. *Arterioscler Thromb Vasc Biol* 2011;31:2493–9. doi:10.1161/ATVBAHA.111.236075.
- [23] Llucià-Valldeperas A, Soler-Botija C, Gálvez-Montón C, Roura S, Prat-Vidal C, Perea-Gil I, et al. Electromechanical Conditioning of Adult Progenitor Cells Improves Recovery of Cardiac Function After Myocardial Infarction. *Stem Cells Transl Med* 2017. doi:10.5966/sctm.2016-0079.
- [24] Julve J, Escolà-Gil JC, Rotllan N, Fiévet C, Vallez E, de la Torre C, et al. Human Apolipoprotein A-II Determines Plasma Triglycerides by Regulating Lipoprotein Lipase Activity and High-Density Lipoprotein Proteome. *Arterioscler Thromb Vasc Biol* 2010;30:232 LP – 238.
- [25] Revuelta-López E, Cal R, Herraiz-Martínez A, de Gonzalo-Calvo D, Nasarre L, Roura S, et al. Hypoxia-driven sarcoplasmic/endoplasmic reticulum calcium ATPase 2 (SERCA2) downregulation depends on low-density lipoprotein receptor-related protein 1 (LRP1)-signalling in cardiomyocytes. *J Mol Cell Cardiol* 2015;85. doi:10.1016/j.yjmcc.2015.04.028.
- [26] Samouillan V, Revuelta-López E, Dandurand J, Nasarre L, Badimon L, Lacabanne C, et al. Cardiomyocyte intracellular cholesteryl ester accumulation

- promotes tropoelastin physical alteration and degradation: Role of LRP1 and cathepsin S. *Int J Biochem Cell Biol* 2014;55. doi:10.1016/j.biocel.2014.09.005.
- [27] Nguyen TD, Carrascal M, Vidal-Cortes O, Gallardo O, Casas V, Gay M, et al. The phosphoproteome of human Jurkat T cell clones upon costimulation with anti-CD3/anti-CD28 antibodies. *J Proteomics* 2016;131:190–8. doi:https://doi.org/10.1016/j.jprot.2015.10.029.
- [28] Óscar G, David O, Marina G, Montserrat C, Joaquin A. A collection of open source applications for mass spectrometry data mining. *Proteomics* 2014;14:2275–9. doi:10.1002/pmic.201400124.
- [29] Chen S, Sen S, Young D, Wang W, Moravec CS, Wu Q. Protease corin expression and activity in failing hearts. *Am J Physiol Hear Circ Physiol* 2010;299:H1687-92. doi:10.1152/ajpheart.00399.2010.
- [30] Orellana-Gavaldà JM, Herrero L, Malandrino Maria I, Pañeda A, Sol Rodríguez-Peña M, Petry H, et al. Molecular therapy for obesity and diabetes based on a long-term increase in hepatic fatty-acid oxidation. *Hepatology* 2010;53:821–32. doi:10.1002/hep.24140.
- [31] Herrero L, Rubí B, Sebastián D, Serra D, Asins G, Maechler P, et al. Alteration of the malonyl-CoA/carnitine palmitoyltransferase I interaction in the β -cell impairs glucose-induced insulin secretion. *Diabetes* 2005;54:462–71. doi:10.2337/diabetes.54.2.462.
- [32] Rebollo A, Roglans N, Baena M, Sánchez RM, Merlos M, Alegret M, et al. Liquid fructose downregulates Sirt1 expression and activity and impairs the oxidation of fatty acids in rat and human liver cells. *Biochim Biophys Acta - Mol Cell Biol Lipids* 2014;1841:514–24. doi:https://doi.org/10.1016/j.bbalip.2014.01.002.
- [33] Pemberton CJ, Siriwardena M, Kleffmann T, Ruygrok P, Palmer SC, Yandle TG, et al. First identification of circulating prepro-A-type natriuretic peptide (preproANP) signal peptide fragments in humans: Initial assessment as cardiovascular biomarkers. *Clin Chem* 2012;58:757–67. doi:10.1373/clinchem.2011.176990.
- [34] Gladysheva IP, Robinson BR, Houg AK, Kováts T, King SM. Corin is co-expressed with pro-ANP and localized on the cardiomyocyte surface in both zymogen and catalytically active forms. *J Mol Cell Cardiol* 2008;44:131–42.

doi:10.1016/j.yjmcc.2007.10.002.

- [35] Schönke M, Massart J, Zierath JR. Effects of high-fat diet and AMP-activated protein kinase modulation on the regulation of whole-body lipid metabolism. *J Lipid Res* 2018;59:1276–82. doi:10.1194/jlr.d082370.
- [36] Viollet B. AMPK: Lessons from transgenic and knockout animals. *Front Biosci* 2009;Volume:19. doi:10.2741/3229.
- [37] Strickland DK, Muratoglu SC, Antalis TM. Serpin–Enzyme Receptors: LDL Receptor-Related Protein 1. *Methods Enzymol* 2011;499:17–31. doi:10.1016/B978-0-12-386471-0.00002-X.
- [38] Gettins PGW, Dolmer K. The high affinity binding site on plasminogen activator inhibitor-1 (PAI-1) for the low density lipoprotein receptorrelated protein (LRP1) Is composed of four basic residues. *J Biol Chem* 2016;291:800–12. doi:10.1074/jbc.M115.688820.
- [39] Ogawa Y, Nakao K, Mukoyama M, Hosoda K, Shirakami G, Arai H, et al. Natriuretic peptides as cardiac hormones in normotensive and spontaneously hypertensive rats: The ventricle is a major site of synthesis and secretion of brain natriuretic peptide. *Circ Res* 1991. doi:10.1161/01.RES.69.2.491.
- [40] Nakao K, Ogawa Y, Suga SI, Imura H. Molecular biology and biochemistry of the natriuretic peptide system. I: Natriuretic peptides. *J Hypertens* 1992. doi:10.1097/00004872-199210000-00002.
- [41] Zhou Y, Wu Q. Corin in Natriuretic Peptide Processing and Hypertension. *Curr Hypertens Rep* 2014;16:415. doi:10.1007/s11906-013-0415-7.
- [42] Luchner A, Muders F, Dietl O, Friedrich E, Blumberg F, Protter AA, et al. Differential expression of cardiac ANP and BNP in a rabbit model of progressive left ventricular dysfunction. *Cardiovasc Res* 2001;51:601–7.
- [43] Toldo S, Austin D, Mauro AG, Mezzaroma E, Van Tassell BW, Marchetti C, et al. Low-Density Lipoprotein Receptor–Related Protein-1 Is a Therapeutic Target in Acute Myocardial Infarction. *JACC Basic to Transl Sci* 2017;2:561–74. doi:10.1016/j.jacbts.2017.05.007.
- [44] Boucher P, Liu P, Gotthardt M, Hiesberger T, Anderson RGW, Herz J. Platelet-derived growth factor mediates tyrosine phosphorylation of the cytoplasmic

- domain of the low density lipoprotein receptor-related protein in caveolae. *J Biol Chem* 2002. doi:10.1074/jbc.M200428200.
- [45] Forte M, Madonna M, Schiavon S, Valenti V, Versaci F, Zoccai GB, et al. Cardiovascular Pleiotropic Effects of Natriuretic Peptides. *Int J Mol Sci* 2019. doi:10.3390/ijms20163874.
- [46] Sengenès C, Zakaroff-Girard A, Moulin A, Berlan M, Bouloumié A, Lafontan M, et al. Natriuretic peptide-dependent lipolysis in fat cells is a primate specificity. *Am J Physiol Integr Comp Physiol* 2002;283:R257–65. doi:10.1152/ajpregu.00453.2001.
- [47] Bartels ED, Guo S, Kousholt BS, Larsen JR, Hasenkam JM, Burnett J, et al. High doses of ANP and BNP exacerbate lipolysis in humans and the lipolytic effect of BNP is associated with cardiac triglyceride content in pigs. *Peptides* 2019. doi:10.1016/j.peptides.2018.11.003.
- [48] Moro C, Klimcakova E, Lolmède K, Berlan M, Lafontan M, Stich V, et al. Atrial natriuretic peptide inhibits the production of adipokines and cytokines linked to inflammation and insulin resistance in human subcutaneous adipose tissue. *Diabetologia* 2007. doi:10.1007/s00125-007-0614-3.
- [49] Engeli S, Birkenfeld AL, Badin PM, Bourlier V, Louche K, Viguerie N, et al. Natriuretic peptides enhance the oxidative capacity of human skeletal muscle. *J Clin Invest* 2012. doi:10.1172/JCI64526.
- [50] Tateya S, Rizzo-De Leon N, Handa P, Cheng AM, Morgan-Stevenson V, Ogimoto K, et al. VASP increases hepatic fatty acid oxidation by activating AMPK in mice. *Diabetes* 2013;62:1913–22. doi:10.2337/db12-0325.
- [51] Schonke M, Massart J, Zierath JR. Effects of high-fat diet and AMPK modulation on the regulation of whole-body lipid metabolism. *J Lipid Res* 2018. doi:10.1194/jlr.D082370.
- [52] Carling D. AMPK signalling in health and disease. *Curr Opin Cell Biol* 2017;45:31–7. doi:10.1016/j.ceb.2017.01.005.
- [53] Lyons CL, Roche HM. Nutritional modulation of AMPK-impact upon metabolic-inflammation. *Int J Mol Sci* 2018;19. doi:10.3390/ijms19103092.
- [54] Herzig S, Shaw RJ. AMPK: Guardian of metabolism and mitochondrial

- homeostasis. *Nat Rev Mol Cell Biol* 2018. doi:10.1038/nrm.2017.95.
- [55] Bu SY, Mashek MT, Mashek DG. Suppression of long chain acyl-CoA synthetase 3 decreases hepatic de Novo fatty acid synthesis through decreased transcriptional activity. *J Biol Chem* 2009. doi:10.1074/jbc.M109.036665.
- [56] Foster DW. The role of the carnitine system in human metabolism. *Ann. N. Y. Acad. Sci.*, 2004. doi:10.1196/annals.1320.001.
- [57] Foretz M, Even PC, Viollet B. AMPK activation reduces hepatic lipid content by increasing fat oxidation in vivo. *Int J Mol Sci* 2018. doi:10.3390/ijms19092826.
- [58] Stefanovic-Racic M, Perdomo G, Mantell BS, Sipula IJ, Brown NF, O'Doherty RM. A moderate increase in carnitine palmitoyltransferase 1a activity is sufficient to substantially reduce hepatic triglyceride levels. *Am J Physiol Metab* 2008;294:E969–77. doi:10.1152/ajpendo.00497.2007.
- [59] Postic C, Dentin R, Girard J. Role of the liver in the control of carbohydrate and lipid homeostasis. *Diabetes & Metab* 2004;858:398 YP – 477. doi:http://dx.doi.org/DM-11-2004-30-5-1262-3636-101019-ART1.
- [60] Sebastián D, Hernández-Alvarez MI, Segalés J, Sorianello E, Muñoz JP, Sala D, et al. Mitofusin 2 (Mfn2) links mitochondrial and endoplasmic reticulum function with insulin signaling and is essential for normal glucose homeostasis. *Proc Natl Acad Sci U S A* 2012. doi:10.1073/pnas.1108220109.
- [61] Bayés-Genís A, Barallat J, Galán A, De Antonio M, Domingo M, Zamora E, et al. Soluble neprilysin is predictive of cardiovascular death and heart failure hospitalization in heart failure patients. *J Am Coll Cardiol* 2015;65:657–65. doi:10.1016/j.jacc.2014.11.048.
- [62] Bayés-Genís A, Barallat J, Pascual D, Nuñez J, Miñana G, Sánchez-Mas J, et al. Prognostic Value and Kinetics of Soluble Neprilysin in Acute Heart Failure. A Pilot Study. *JACC Hear Fail* 2015;3:641–4. doi:10.1016/j.jchf.2015.03.006.
- [63] Sengenès C, Bouloumié A, Hauner H, Berlan M, Busse R, Lafontan M, et al. Involvement of a cGMP-dependent pathway in the natriuretic peptide-mediated hormone-sensitive lipase phosphorylation in human adipocytes. *J Biol Chem* 2003;278:48617–26. doi:10.1074/jbc.M303713200.
- [64] Birkenfeld AL, Budziarek P, Boschmann M, Moro C, Adams F, Franke G, et al.

Atrial Natriuretic Peptide Induces Postprandial Lipid Oxidation in Humans. *Diabetes* 2008;57:3199–204. doi:10.2337/db08-0649.

- [65] Moro C, Crampes F, Sengenès C, De glisezinski I, Galitzky J, Thalamas C, et al. Atrial natriuretic peptide contributes to physiological control of lipid mobilization in humans. *FASEB J* 2004;18:908–10. doi:10.1096/fj.03-1086fje.
- [66] Chainani-Wu N, Weidner G, Purnell DM, Frenda S, Merritt-Worden T, Kemp C, et al. Relation of B-Type Natriuretic Peptide Levels to Body Mass Index After Comprehensive Lifestyle Changes. *Am J Cardiol* 2010;105:1570–6. doi:10.1016/j.amjcard.2010.01.016.
- [67] Chen-Tournoux A, Khan AM, Baggish AL, Castro VM, Semigran MJ, McCabe EL, et al. Impact of Weight Loss Following Weight Loss Surgery on Levels of Plasma N-Terminal Pro-B-Type Natriuretic Peptide. *Am J Cardiol* 2010;106:1450–5. doi:10.1016/j.amjcard.2010.06.076.

Figure Legends

Figure 1. *cm-Lrp1*^{-/-} Transgenic Mice Generation and Validation

(A) Generation schedule of an *in vivo* model with a doxycycline-inducible attenuation of *Lrp1* expression selectively in cardiomyocytes. In *cm-Lrp1*^{-/-} mice with the genotype TnTCre^{+/+} *Lrp1*^{fllox/fllox}, the activation of Cre recombinase by doxycycline converts the *Lrp1* floxed alleles to KO (-) alleles. (B) Cre and Flox transgens were detected by PCR. A fragment of 500 bp was amplified from mouse tail genomic DNA when the Cre transgene driven by the TnT promoter was present. A fragment of 350 bp was amplified when flox sequences flank *Lrp1* gen. (C) Ten-week-old male mice were treated daily with doxycycline cyclate through their drinking water during the procedure to assess the conditional inhibition of LRP1 levels in cardiomyocytes. After three days of treatment, both *cm-Lrp1*^{+/+} and *cm-Lrp1*^{-/-} mice were randomized and fed a chow diet or high fat diet for six weeks. (D) *Lrp1* mRNA expression and LRP1 protein levels (in green) in isolated cardiomyocytes from hearts of *cm-Lrp1*^{-/-} and control mice (E) *Lrp1* mRNA expression and LRP1 protein levels (LRP1 staining in red, nuclei in blue, Bar=20 μm) in the heart. Data represent the mean±SEM for 9 mice per group. *** p<0.005 versus *cm-Lrp1*^{+/+} mice; ### p<0.005 versus chow diet. Differences between groups were analyzed using one-way analysis of variance (ANOVA) followed by a post-hoc Tukey-b test.

Figure 2. *Lrp1* Deficiency in Cardiomyocytes Improves Diet-induced Glucose Intolerance and Reduces Weight Gain

cm-Lrp1^{+/+} and *cm-Lrp1^{-/-}* mice (control) mice were treated for 6 weeks with doxycycline cyclate in their drinking water. (A) Body weight changes over 6 weeks of HFD diet. (B) Epididymal white adipose tissue (eWAT) tissue mass at necropsy. (C) Representative H&E stained sections from eWAT and brown adipose tissue (BAT) (Bar=100 μ m). (D) Triglyceride and FA content in the liver and representative Herxheimer stained liver sections (Bar =100 μ m). (E) Glucose tolerance test in mice (1.3 mg/g body weight) and Area under the curve (AUC). The data represents the mean \pm SEM. n=9 mice per condition. **p<0.01 or *** p<0.005 *versus* control mice. Differences between groups were analyzed using Student's t test for independent samples.

Figure 3. Cardiomyocyte *Lrp1* Deficiency Increases Whole-Body Energy Consumption

cm-Lrp1^{+/+} and *cm-Lrp1^{-/-}* mice (control) mice were treated for 6 weeks with doxycycline cyclate in their drinking water and then submitted to CLAMS experiments. Oxymax respirometer measurements of lipid oxidation (A), glucose oxidation (B), VO₂ (C) and whole-body oxygen consumption (D) during the light and dark periods in mice over 6 weeks on HFD. n=8 mice per condition. *p<0.05, **p<0.01 or ***p<0.005 *versus cm-Lrp1^{+/+}* mice. Differences between groups were analyzed using Student's t test for independent samples.

Figure 4. Cardiomyocyte *Lrp1* Deficiency Favors Higher Corin Activity and ANP Release

(A) Schematic representation for the secretion of preproANP-derived peptides modified from Pemberton et al [23]. The AA sequence RIGAQSGLCNSFR that is recognized by the antibody (Ab) is localized at the extreme C-terminal of the protein. *cm-Lrp1^{+/+}* and *cm-Lrp1^{-/-}* mice (control) mice were treated for 6 weeks with doxycycline cyclate in their drinking water. After sacrifice, one aliquote of frozen heart tissue was used for protein extraction. (B) Representative Western blot analysis showing cardiac preproANP (16 kDa), proANP (13 kDa) and troponin (TnT) (endogenous control) protein bands and bar graphs showing the quantification of preproANP and proANP protein bands normalized to TnT. One aliquot of cardiac membranes (5 mg) was used for immunoprecipitation with anti-corin Abs. (C) Immunoblots performed with anti-SerpinA1 Abs showing two different molecular weight corin/serpinA1 complexes and bar graphs showing the quantification of 45-50 kDa complex and 30-35 kDa complex.

(D) Other aliquot of cardiac membranes (25 μ g) was used for membrane protease catalytic activity measurements (V_{max}) in absence or presence of the thrombin inhibitor hirudin (2 μ M). (E-G) Circulating levels of ANP, adrenalin/epinephrine and GDF15 measured by ELISA. $n=6$ mice per condition. Data represent the mean \pm SEM. ** $p<0.01$ or *** $p<0.005$ versus *cm-Lrp1^{+/-}* mice. Differences between groups were analyzed using Student's t test for independent samples.

Figure 5. High Plasma ANP Levels in *cm-Lrp1^{-/-}* Mice Induce NPRA-Dependent Signaling Linked to AMPK Phosphorylation and Increased Fatty Acid Oxidation in the Liver

cm-Lrp1^{+/+} and *cm-Lrp1^{-/-}* mice (control) mice were treated for 6 weeks with doxycycline cyclate in their drinking water and then treated with either saline or the NPRA antagonist A71915 (200 μ g/kg in PBS in a final volume of 100 μ l) for the last 4 weeks. (A) cGMP levels were detected by ELISA. Western blot analysis and bar graphs showing the quantification of pVASP, total VASP, pAMPK, total AMPK, pACC and total ACC (B) and OXPHOS, UCP3 and CPT1 (C) in the liver. (D) Rate of hepatic fatty acid oxidation (FAO). (E) Representative Herxheimer stained liver sections (Bar =100 μ m) and hepatic TG levels. $n=8-10$ mice per condition. Data represent the mean \pm SEM. * $p<0.05$, ** $p<0.01$ or *** $p<0.005$ versus *cm-Lrp1^{+/+}* mice; ## $p<0.01$ or ### $p<0.005$ vs PBS. Differences between groups were analyzed using one-way analysis of variance (ANOVA) followed by a post-hoc Tukey-b test.

Figure 6. Hepatocytes Exposed to Supernatants from LRP1-deficient (LRP1-) HL-1 Cardiomyocytes Exhibited Increased Levels of Phosphorylated AMPK and CPT1

LRP1 deficient HL-1 (LRP1-) and control HL-1 cells (LRP1+) were grown in complete Claycomb medium from 48 hours and supernatants were then collected. After determination of their ANP content by ELISA, supernatants were directly added to cultured hepatocytes (Hepa 1-6). Hepa 1-6 were exposed to HL-1 supernatants for 18 hours and then collected in lysis buffer to perform Western blot analysis. (A) Representative optical microscopy image of LRP1+ and LRP1- HL-1 cells. (B) Western blot analysis and bar graphs showing LRP1 protein levels in LRP1- compared to LRP1+ HL-1 cells. (C) ANP levels in LRP1+ and LRP1- supernatants measured by ELISA. (D) Representative optical microscopy image of Hepa 1-6 cells exposed to supernatants from LRP1+ and LRP1- HL-1 cells. (E) Western blot analysis and bar graphs showing pAMPK/total AMPK ratio and CPT1 protein levels of Hepa 1-6. Data

represent the mean \pm SEM of three experiments performed in duplicate. ** $p < 0.01$ or *** $p < 0.005$ versus LRP1+ HL-1 cells or versus Hepa 1-6 cells exposed to supernatants from control HL-1 cells. Differences between groups were analyzed using Student's t test for independent samples.

Figure 7. TG and FA Uptake Increased in the Liver while Decreased in eWAT of *cm-Lrp1*^{-/-} Mice

cm-Lrp1^{+/+} and *cm-Lrp1*^{-/-} mice (control) mice were treated for 6 weeks with doxycycline cyclate in their drinking water and then treated with either saline or the NPR-A antagonist A71915 for the last 4 weeks. Mice were then given an oral fat gavage (OFG) consisting of 20 μ Ci [³H]-labeled triolein in 150 μ L of olive oil as. Percentage of [³H]-triglyceride and [³H]-free fatty acid uptake by liver (A) and eWAT (B) in the different groups taking as reference the control group. Real-time PCR of *Vldlr* and *Cd36* mRNA expression levels in liver (C) and eWAT (D). (E) Representative Herxheimer stained eWAT sections (Bar =100 μ m). Data represent the mean \pm SEM. * $p < 0.05$, ** $p < 0.01$ or *** $p < 0.005$ versus control mice; ## $p < 0.01$ or ### $p < 0.005$ versus PBS. Differences between groups were analyzed using one-way analysis of variance (ANOVA) followed by a post-hoc Tukey-b test.

Figure 8. Cardiomyocyte *Lrp1* Deficiency Increases Whole-Body Energy Consumption in an NPR-A Dependent manner

cm-Lrp1^{+/+} and *cm-Lrp1*^{-/-} mice (control) mice were treated for 6 weeks with doxycycline cyclate in their drinking water and then treated with either saline or the NPR-A antagonist A71915 for the last 4 weeks. OxyMax respirometer measurements of lipid oxidation (A), glucose oxidation (B) VO_2 (C) and whole-body oxygen consumption (D) during the light and dark periods. $n = 8-10$ mice per condition. * $p < 0.05$, ** $p < 0.01$ or *** $p < 0.005$ versus control mice; ## $p < 0.01$ or ### $p < 0.005$ versus PBS. Differences between groups were analyzed using one-way analysis of variance (ANOVA) followed by a post-hoc Tukey-b test.

Figure 9. Schematic main figure

Cardiomyocyte *Lrp1* deficiency facilitates corin activation and ANP release from the heart. NPR-A/cGMP/pVASP signaling activates AMPK/ACC pathway that coordinately inhibits FA synthesis and activates FA uptake and oxidation in the liver of *cm-Lrp1*^{-/-} mice. The ANP-mediated activation of AMPK seems to underlie the decrease in

hepatic TG content, the improved glucose tolerance, the limited weight gain and the enhanced whole-body energy consumption of cardiomyocyte-*Irp1* deficient mice.

Table 1. Comparison of serum glucose levels, serum insulin levels and Homeostatic Model Assessment for Insulin Resistance (HOMA-IR) between *cm-Lrp1^{-/-}* and control mice. The data is shown as mean±SEM. N=8 per group. Differences between groups were analyzed using the Student's t test for independent samples.

| | <i>cm-Lrp1^{+/+}</i> | <i>cm-Lrp1^{-/-}</i> | <i>P</i> |
|-----------------------|------------------------------|------------------------------|----------|
| GLUCOSE (mM) | 11.09 ± 0.37 | 9.49 ± 0.84 | 0.072 |
| INSULIN (µg/L) | 1.23 ± 0.17 | 0.48 ± 0.04 | 0.003 |
| HOMA-IR | 13.06 ± 1.55 | 4.59 ± 0.74 | 0.003 |

Table 2. Differential cardiac secreted proteins between *cm-Lrp1^{-/-}* and *cm-Lrp1^{+/+}* mice. This table shows mass spectrometric proteomic data concerning differential cardiac secreted proteins. Three biological replicates for each condition were processed. Each replicate was a pool of tissue obtained from three different animals. Differences between groups were analyzed using Student's t test for independent samples.

| Protein ID | Protein name | Gene name | <i>cm-Lrp1^{-/-}</i> vs <i>cm-Lrp1^{+/+}</i> | |
|------------|--------------------------------|----------------------------|--|----------|
| | | | Ratio | <i>P</i> |
| E9PV24 | Fibrinogen alpha chain | Fga | 0.64 | 1.8E-12 |
| P05125 | Natriuretic peptides A (ANP) | Nppa Pnd | 0.57 | 4.8E-04 |
| P07759 | Serine protease inhibitor A3K | Serpina3k Mcm2 Spi2 | 0.63 | 1.6E-12 |
| P22599 | Alpha-1-antitrypsin 1-2 | Serpina1b Aat2 Dom2 Spi1-2 | 0.44 | 1.2E-05 |
| Q00897 | Alpha-1-antitrypsin 1-4 | Serpina1d Dom4 Spi1-4 | 0.30 | 9.4E-04 |
| Q3TFQ8 | Alpha-1,4 glucan phosphorylase | Pygb | 0.72 | 8.1E-16 |
| Q6S9I0 | Kininogen | Kng2 | 0.77 | 1.1E-03 |
| P01942 | Hemoglobin subunit alpha | Hba | 0.74 | 9.6E-05 |
| Q8K0E8 | Fibrinogen beta chain | Fgb | 0.66 | 6.6E-14 |
| Q8VCM7 | Fibrinogen gamma chain | Fgg | 0.65 | 5.5E-08 |
| Q91X72 | Hemopexin | Hpx Hpxn | 0.70 | 5.0E-09 |

AUTHOR CONTRIBUTION SECTION

Concept and design: Vicenta Llorente-Cortés and Joan Carles Escola-Gil.

Performed the experiments: Aleyda Benítez-Amaro, Elena Revuelta-López, Olga Bornachea, Lidia Cedo, Angela Vea, Laura Herrero, Nuria Roglans, Carolina Soler-Botija, Jesús Eduardo García, Laura Nasarre, Eugenia Mato, David Sebastian.

Data analysis and interpretation: Vicenta Llorente-Cortés, David de Gonzalo-Calvo, Sandra Camino-López, Francisco Blanco Vaca, Antoni Bayes Genis, Antonio Zorzano, Joan Carles Laguna, Dolors Serra, Joan Carles Escola-Gil, David Sebastian.

Writing and review of Manuscript: Elena Revuelta-López, Joan Carles Escola-Gil, Vicenta Llorente-Cortés.

Journal Pre-proof

HIGHLIGHTS

- Cardiomyocyte *Lrp1* deficiency preserves corin activity and promotes ANP release
- Increased blood ANP levels activate cGMP/pVASP axis in skeletal muscle and liver
- In the liver, but not in skeletal muscle, cGMP/pVASP axis was linked to AMPK phosphorylation and activation
- Increased hepatic pAMPK promotes whole-body systemic energy expenditure

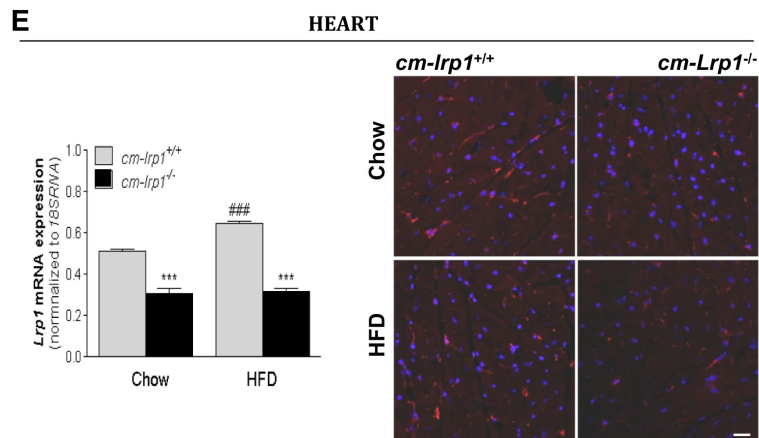
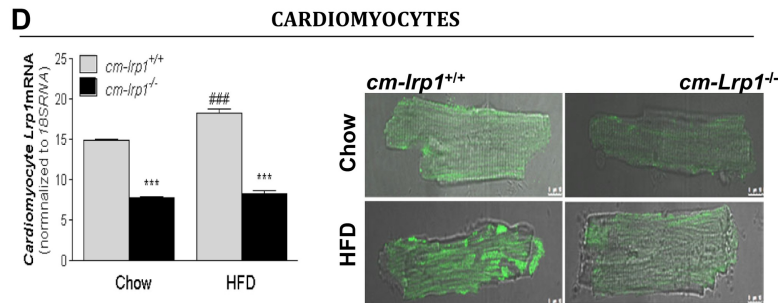
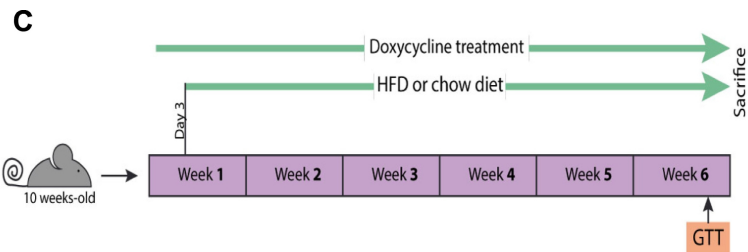
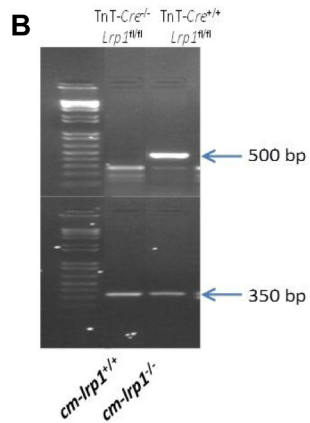
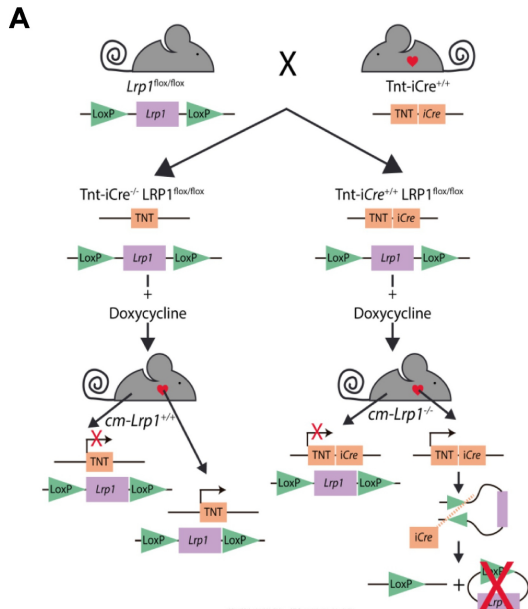


Figure 1

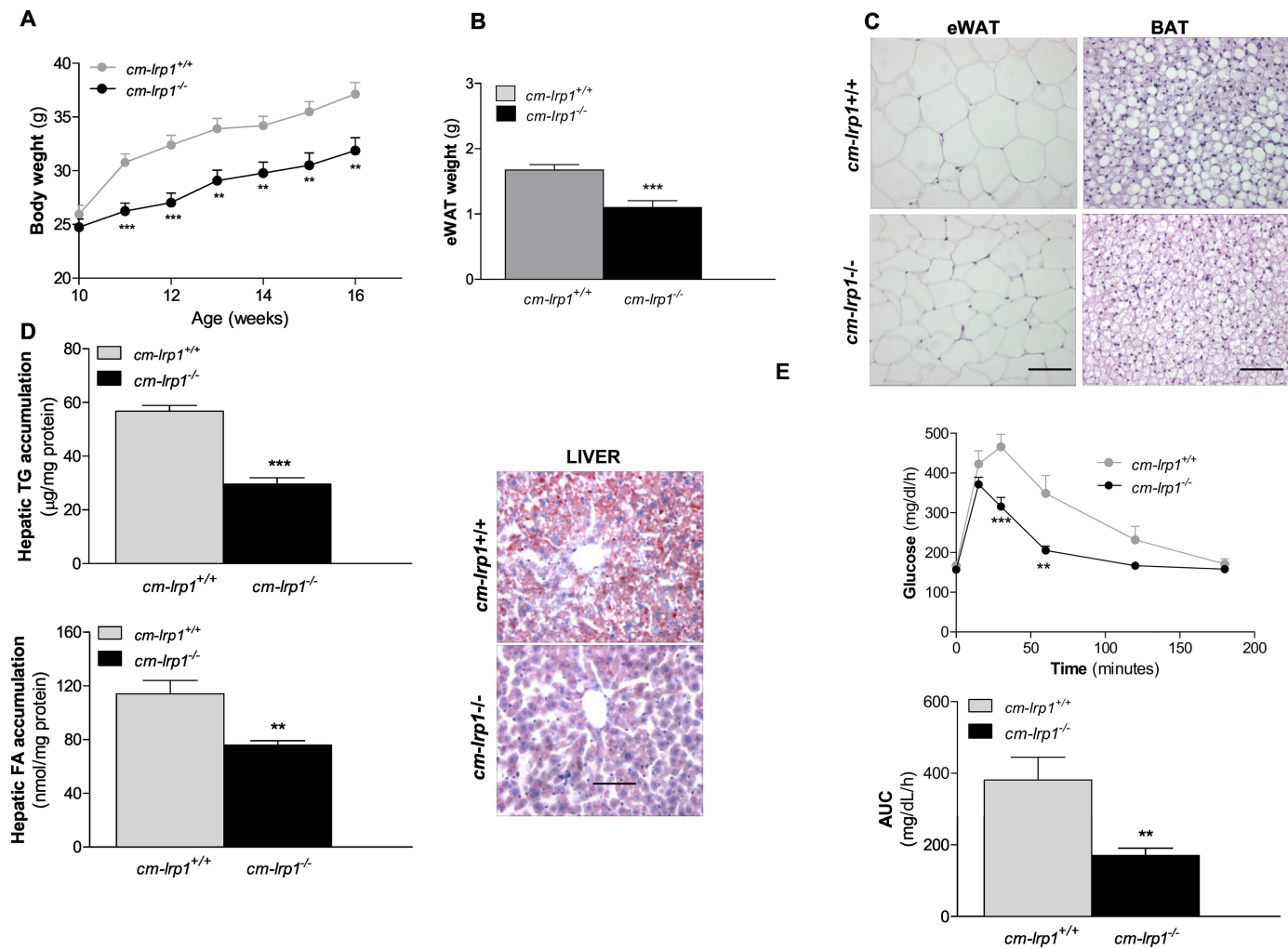


Figure 2

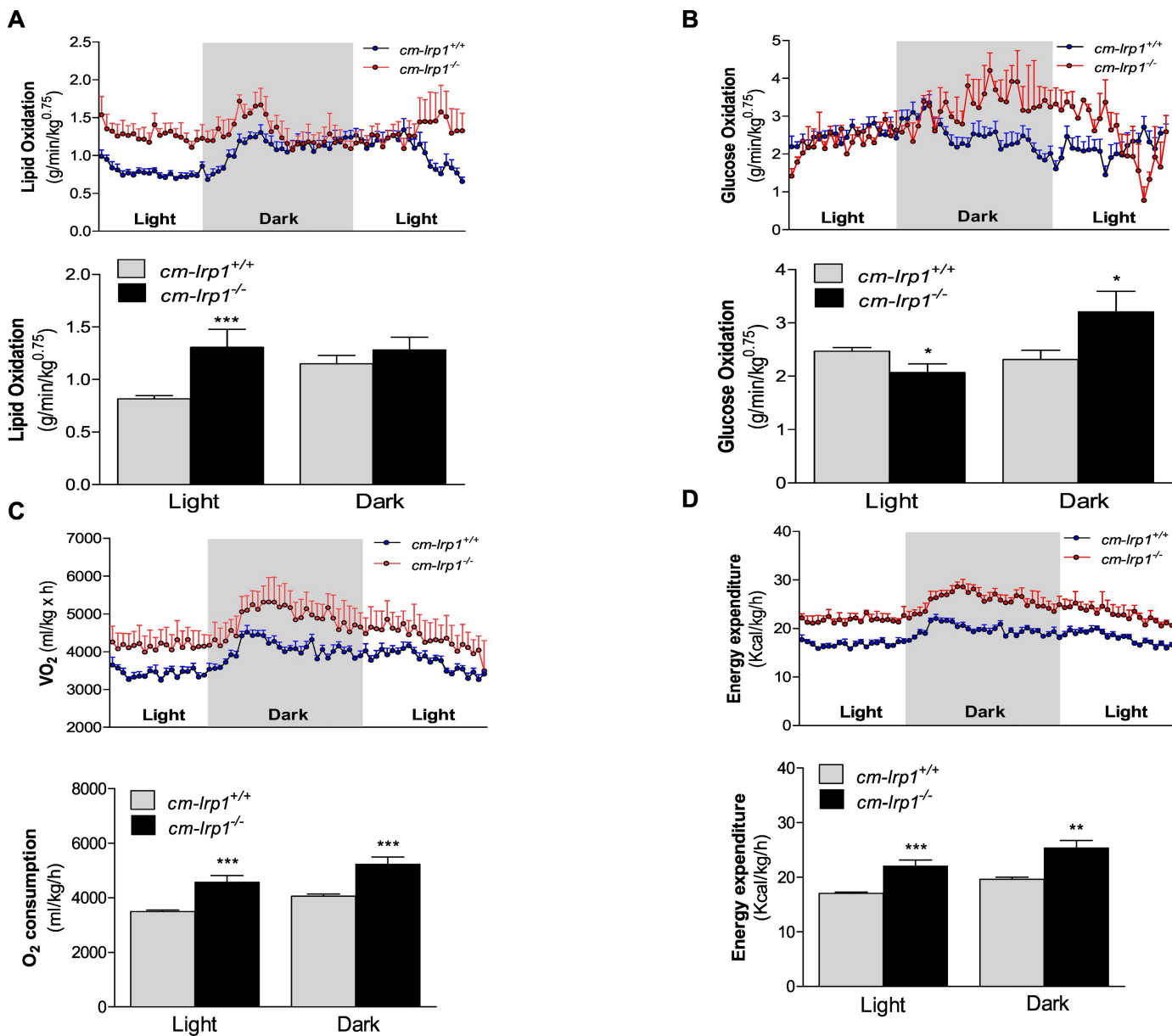


Figure 3

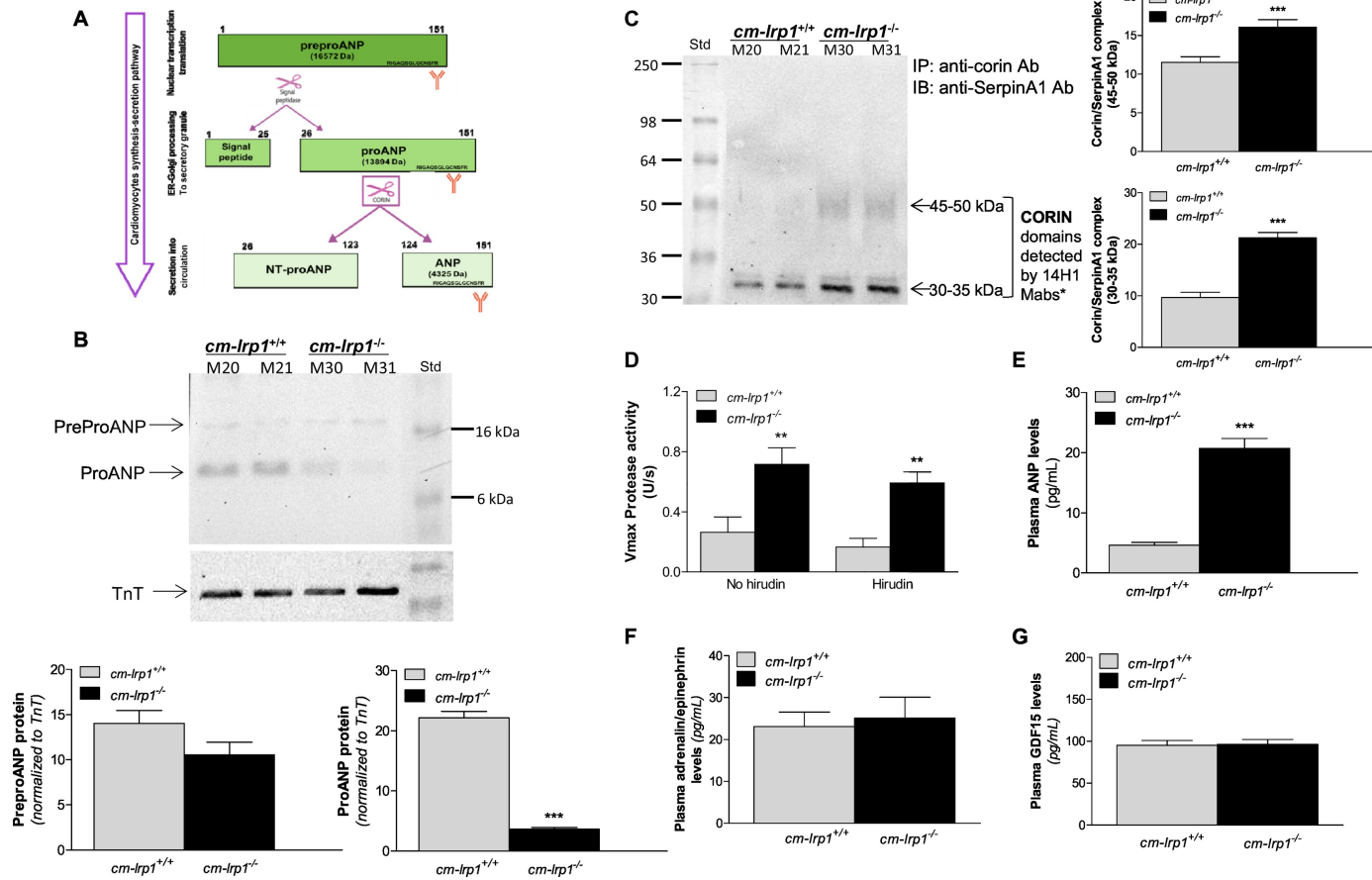


Figure 4

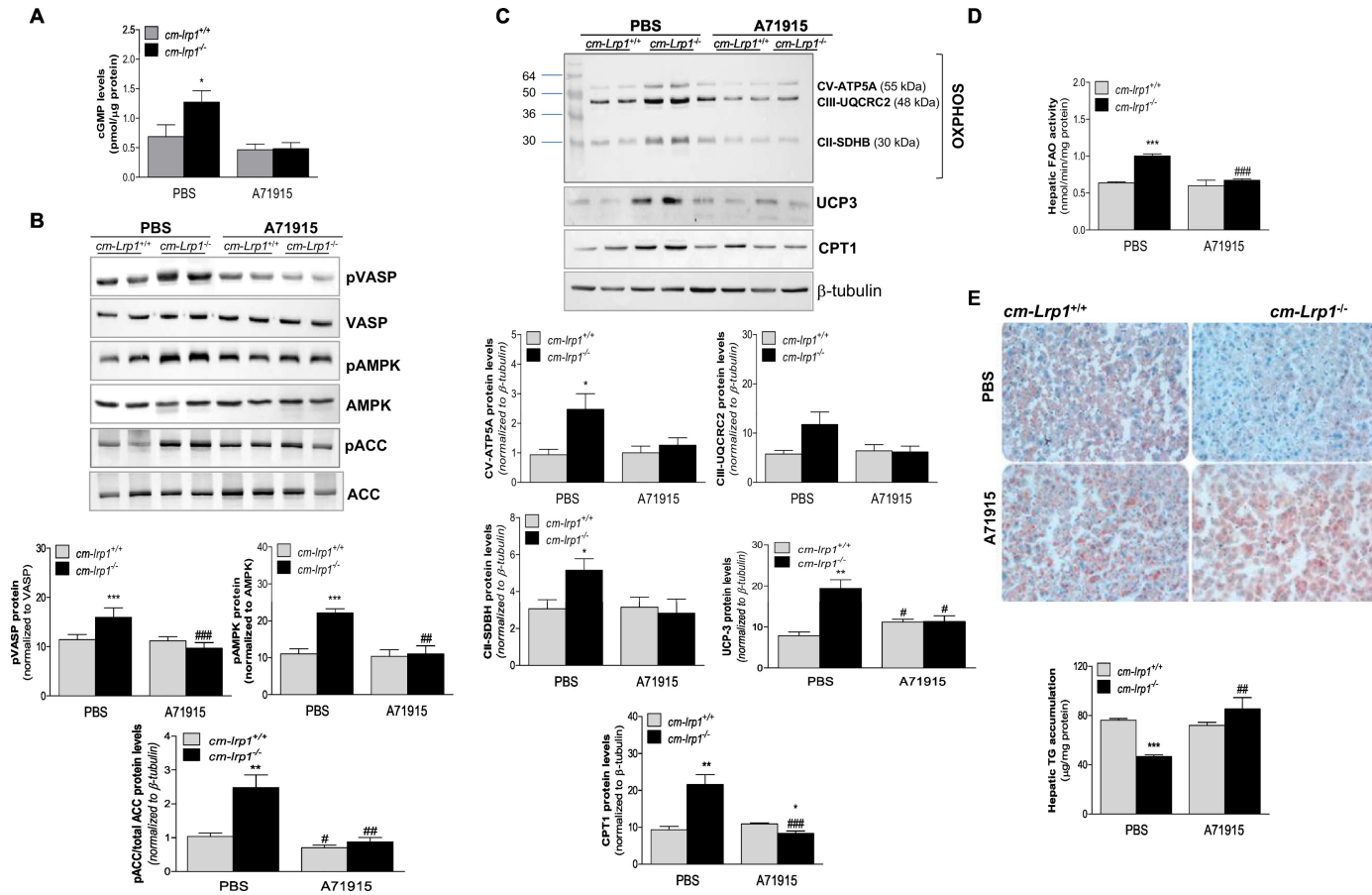


Figure 5

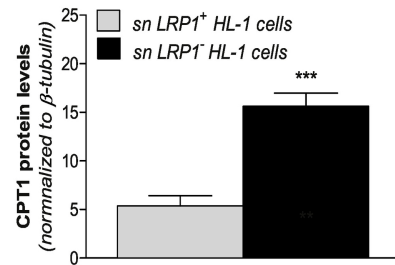
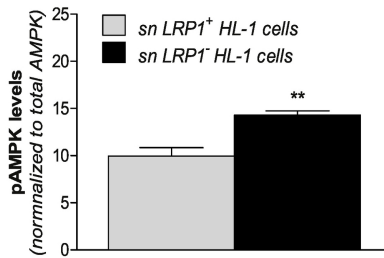
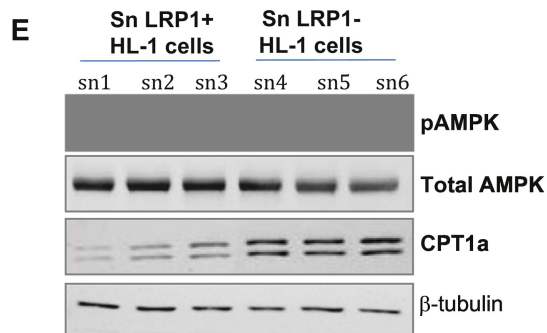
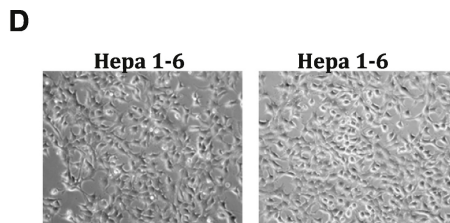
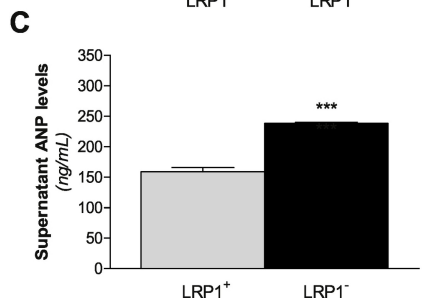
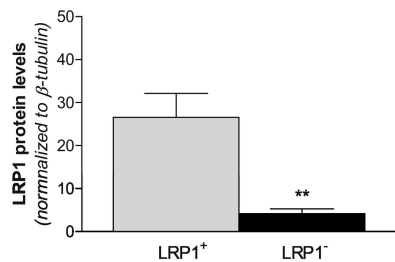
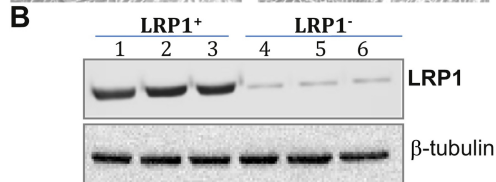
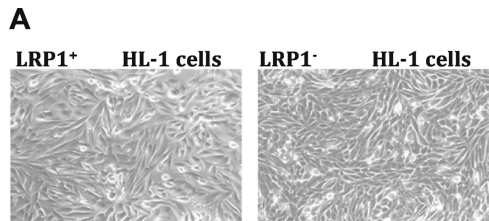
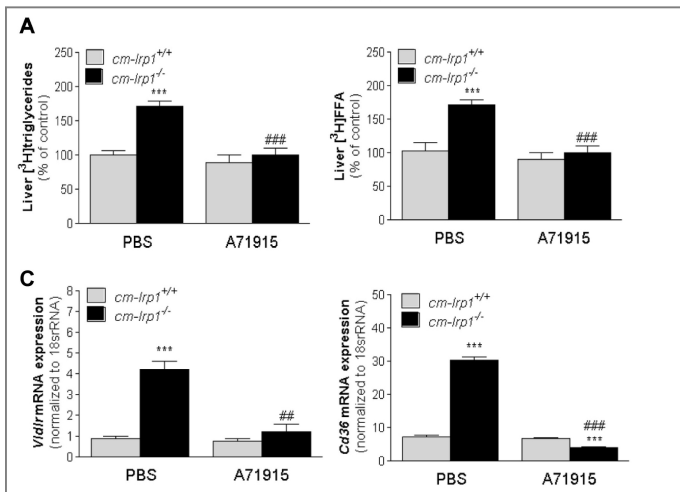
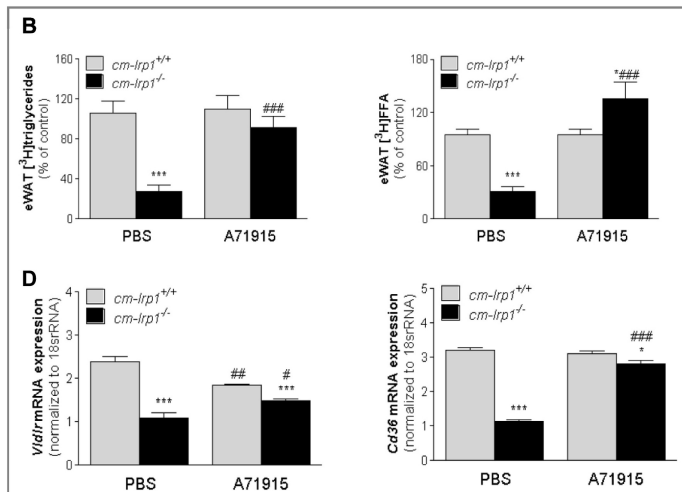


Figure 6

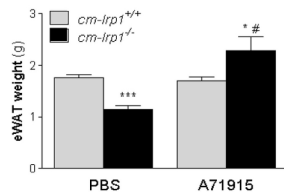
LIVER



eWAT



E



F

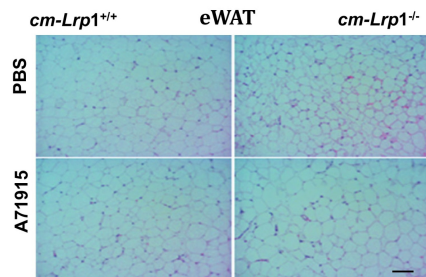


Figure 7

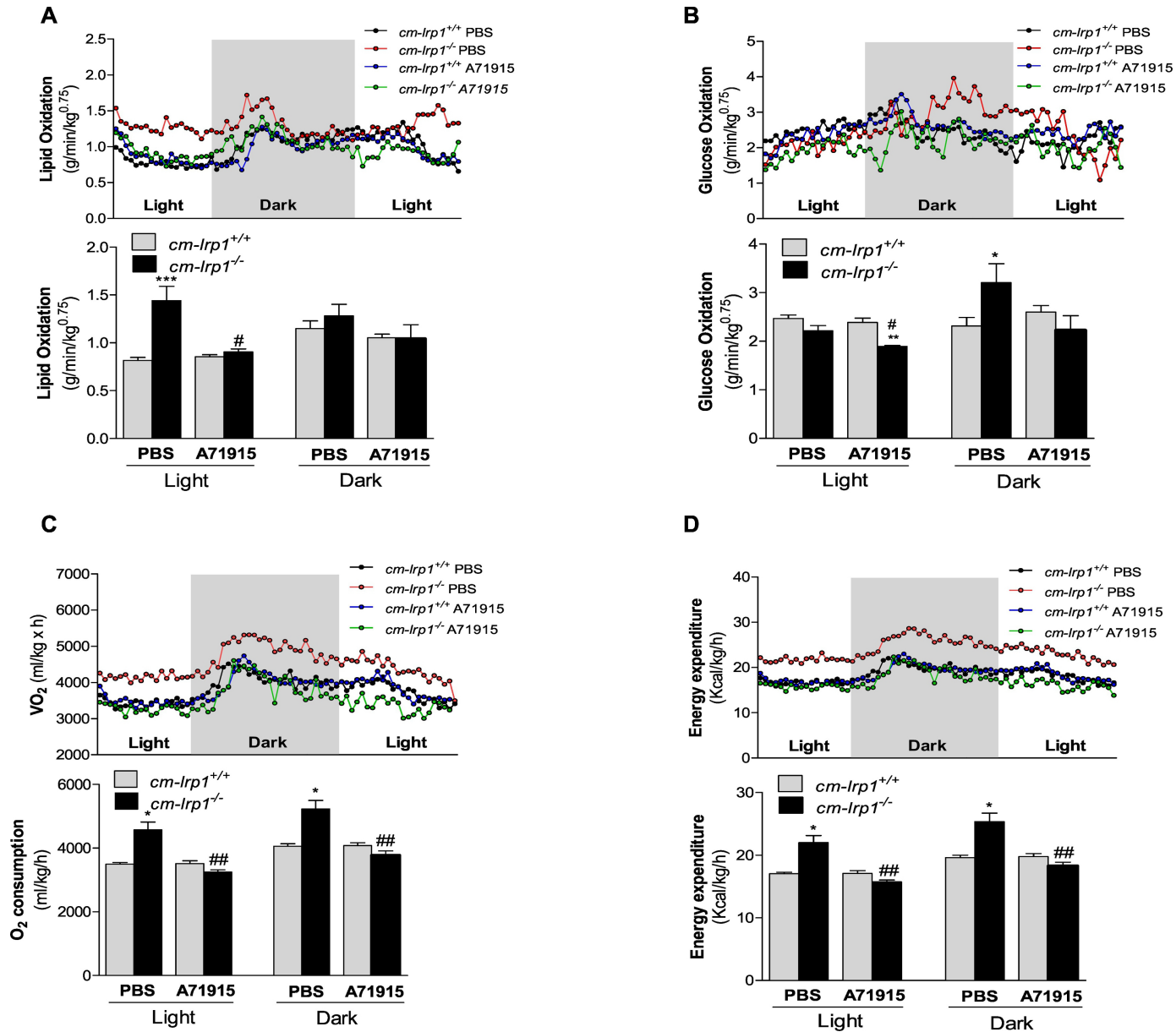


Figure 8

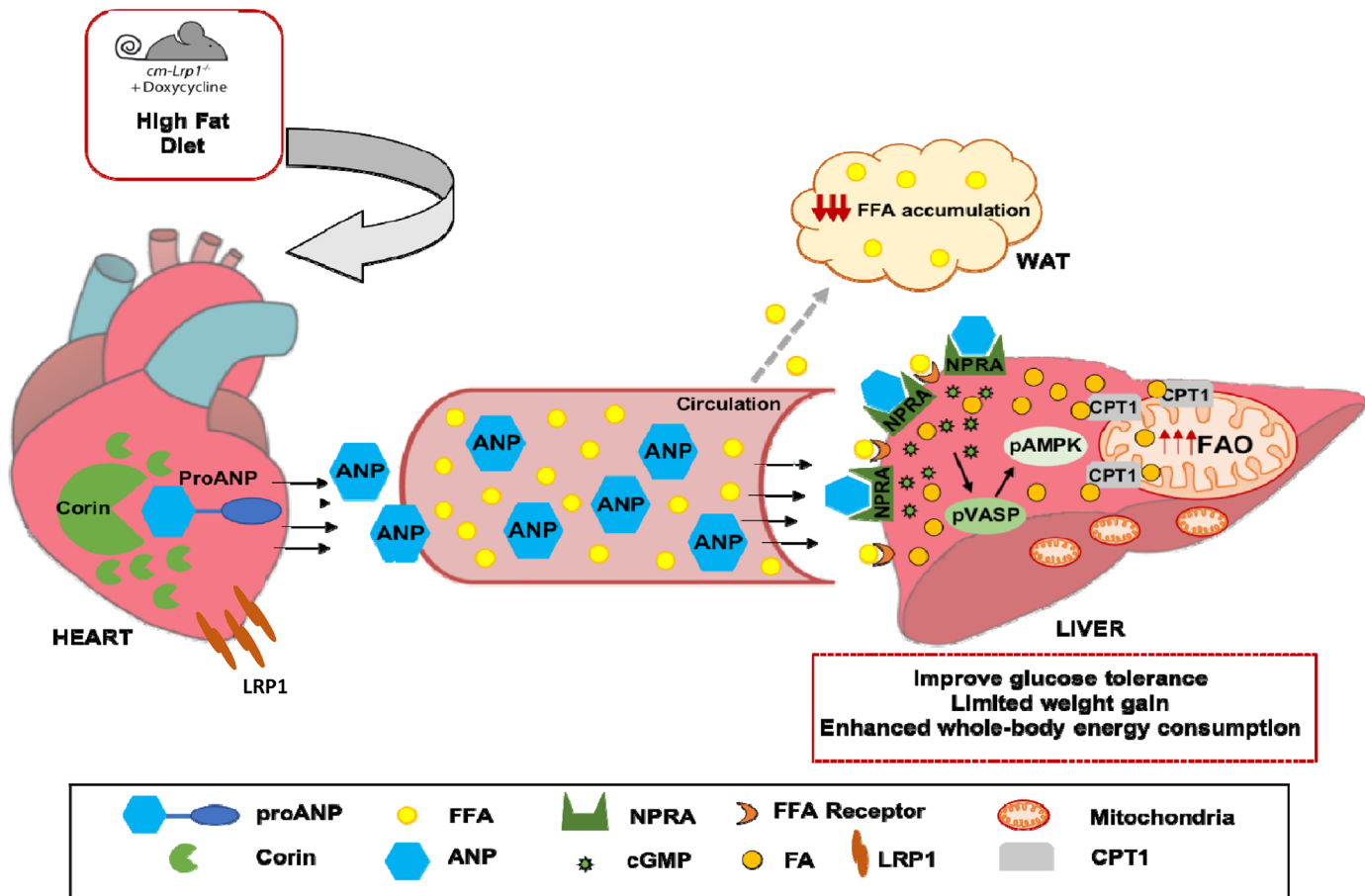


Figure 9